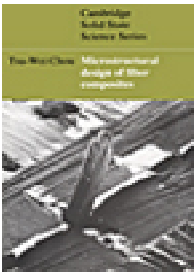

Microstructural Design of Fiber Composites

Tsu-Wei Chou

Book DOI: http://dx.doi.org/10.1017/CBO9780511600272

Online ISBN: 9780511600272

Hardback ISBN: 9780521354820

Paperback ISBN: 9780521019651

Chapter

4 - Short-fiber composites pp. 169-230

Chapter DOI: http://dx.doi.org/10.1017/CBO9780511600272.005

Cambridge University Press

4 Short-fiber composites

4.1 Introduction

Composites reinforced with discontinuous fibers are categorized here as short-fiber composites. The fiber aspect ratio (length/diameter $= l/d$) is often used as a measurement of fiber relative length. Depending upon the dispersion of fibers in the matrix, the relevant d values may include those of the filaments, strands, rovings, as well as other forms of fiber bundles. Although discontinuous fibers such as whiskers have been used to reinforce metals and ceramics, the majority of short-fiber composites are based upon polymeric matrices. Discontinuous fiber-reinforced plastics are attractive in their versatility in properties and relatively low fabrication costs. The concern of the rapid depletion of world resources in metals and the search for energy-efficient materials has contributed to the increasing interest in composite materials. Discontinuous fiber-reinforced plastics will constitute a major portion of the demand of composites in automotive, marine and aeronautic applications.

A discontinuous fiber composite usually consists of relatively short, variable length, and imperfectly aligned fibers distributed in a continuous-phase matrix. In polymeric composites the fibers are mostly glass, although carbon and aramid are also used; non-fibrous fillers are often added. The orientation of the fibers depends upon the processing conditions employed and may vary from random in-plane and partially aligned to approximately uniaxial.

The understanding of the behavior of short-fiber composites is complicated by the non-uniformity in fiber length and orientation as well as the interaction between the fiber and matrix at fiber ends (Chou and Kelly 1976, 1980). These factors are examined in the following discussions on the physical and mechanical properties of short-fiber composites.

4.2 Load transfer

Various attempts have been made to evaluate the stress transfer from the matrix to the fiber in a short-fiber composite. Analyses based upon the shear-lag theory, elasticity theory, and finite element method have been performed. Considerations regarding fiber aspect ratio (Fukuda and Kawata 1974), the effects of bonded ends and loose ends as well as the geometric shapes of fiber ends (Burgel, Perry and Schneider 1970), and the distribution of radial and circumferential stresses near the interface at fiber ends (Haener and Ashbaugh 1967; Carrara and McGarry 1968) have been made. Experimental measurements of interfacial strength have been made using a single fiber pull out test (Favre and Perrin 1972), a fiber fragmentation test (Wadsworth and Spilling 1968), a microtension test (Miller, Muri and Rebenfeld 1987) and a micro-compression test (Mandell, Grande, Tsiang and McGarry 1986). (Also see Piggott 1987 and Piggott and Dai 1988.)

Although the shear-lag approach is not as rigorous as the other methods, it does provide a simplistic analysis for gaining some insights into a complex problem and it will be employed in the following. The fiber axial and interfacial stresses are discussed with or without the consideration of interactions among neighboring short fibers.

4.2.1 *A single short fiber*

Cox (1952) first dealt with the problem of a single short fiber embedded in an infinite matrix material. In this essentially one-dimensional approach the load on the fiber is considered to be built up entirely due to the generation of shear stress in the matrix. Under the assumptions of shear-lag analysis no tensile stress is permitted to transmit across a fiber end.

Consider a long cylindrical composite of radius R which contains a fiber of radius r_o and length l along the cylinder axis. The composite as a whole is subjected to a normal strain ε in the direction of the fiber. The assumption of the shear-lag analysis leads to the following relation:

$$\frac{\mathrm{d}P}{\mathrm{d}x} = H(u - v) \tag{4.1}$$

where $u(x)$ is the displacement of the fiber at the point x; $v(x)$ is the matrix displacement; H is a constant; and P is the fiber axial force. The force–displacement relation of the fiber is

$$P = E_f A_f \frac{\mathrm{d}u}{\mathrm{d}x} \tag{4.2}$$

where E_f and A_f denote the fiber axial Young's modulus and cross-sectional area, respectively. Substituting Eq. (4.2) and $\mathrm{d}v/\mathrm{d}x =$ constant $= \varepsilon$ into Eq. (4.1), and applying the boundary conditions

$P = 0$ at $x = 0$ and l, the fiber axial stress, σ_f, and interfacial shear stress, τ, are obtained:

$$\sigma_f = \frac{P}{A_f} = E_f \varepsilon \left[1 - \frac{\cosh \beta(l/2 - x)}{\cosh (\beta l/2)} \right]$$
$$\tau = E_f \varepsilon \sqrt{\left[\frac{G_m}{2E_f \ln(R/r_o)} \right]} \frac{\sinh \beta(l/2 - x)}{\cosh(\beta l/2)} \tag{4.3}$$

where

$$\beta = \sqrt{[H/E_f A_f]}$$

$$H = \frac{2\pi G_m}{\ln(R/r_o)}$$

Here, G_m and E_f are the matrix shear modulus and fiber Young's modulus, respectively. Figure 4.1 shows schematically the variation of σ_f and τ along the length of the fiber. The largest axial stress in the fiber occurs at the center and it reaches $E_f\varepsilon$ for a very long fiber. The magnitude of τ reaches its maximum at the fiber ends, i.e., at $x = 0$ and l, and it vanishes at the middle point of the fiber.

4.2.2 *Fiber–fiber interactions*

The interactions among fibers in a short-fiber composite are more complex than those in a continuous fiber composite. This is because the axial load carried by a short fiber has to be transferred to the neighboring fibers at locations near its ends. To illustrate the load transfer in a short-fiber composite, the work of Fukuda and Chou (1981a) is recapitulated in the following. This approach, based upon the shear-lag model, introduces axial load into the

Fig. 4.1. The variation of σ_f and τ along a short fiber.

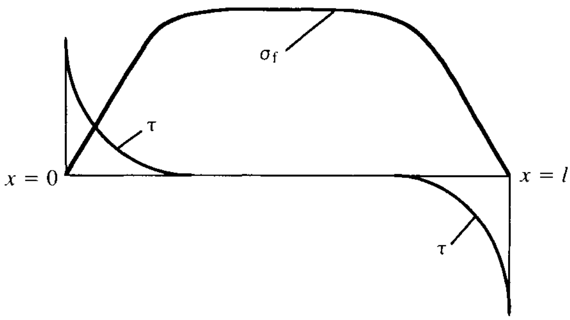

matrix, and the fiber ends are assumed to be bonded to the matrix. These assumptions of the modified shear-lag analysis are valid if the bonding between the fiber and matrix at the fiber end is perfect such as the cases often observed in metal matrix composites and in polymeric matrix composites under compression.

The two-dimensional model for analysis is given in Fig. 4.2, where the hatched parts of the matrix sustain axial load and behave as if they are fibers with a Young's modulus different from the actual fibers. The fiber diameter and matrix layer width are denoted by d and h, respectively. A representative region in Fig. 4.2 containing fiber ends is divided into n parts along the fiber direction x. Fibers in this region are numbered from $i=1$ to $i=m$. Figure 4.3 shows a free body diagram of a fiber and the adjacent matrix. The equilibrium of forces in the x direction gives

$$\frac{\mathrm{d}P_{1j}}{\mathrm{d}x}+\tau_{1j}=0$$

$$\frac{\mathrm{d}P_{ij}}{\mathrm{d}x}+\tau_{ij}-\tau_{i-1j}=0 \qquad (i=2,\ldots,m-1) \tag{4.4}$$

$$\frac{\mathrm{d}P_{mj}}{\mathrm{d}x}-\tau_{m-1j}=0$$

Fig. 4.2. The general model of analyses, $\xi=x/d$. (After Fukuda and Chou 1981a).

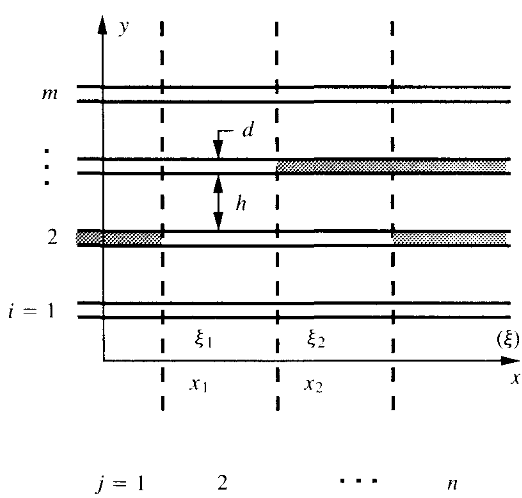

where P_{ij} and τ_{ij} are, respectively, the axial force of the ith fiber and the interfacial shear stress in the jth region. The condition of linear elastic deformation leads to the following stress–strain relations:

$$P_{ij} = E_{ij} d \frac{\mathrm{d}u_{ij}}{dx}$$

$$\tau_{ij} = \frac{G}{h}(u_{i+1j} - u_{ij}). \tag{4.5}$$

where E, G and u denote the Young's modulus of the fiber, shear modulus of the matrix, and displacement of the fiber, respectively. The subscripts i and j indicate the ith fiber and jth region as shown in Fig. 4.2. Thus, E_{ij} is either E_f (Young's modulus of the fiber) or E_m (Young's modulus of the matrix).

The above general formulation is now applied to a model composite shown in Fig. 4.4. This model is composed of a row of short fibers of equal length and two surrounding long fibers. This simple model is adopted for demonstrating the load transfer of short

Fig. 4.3. Free body diagram of the ith fiber. (After Fukuda and Chou 1981a.)

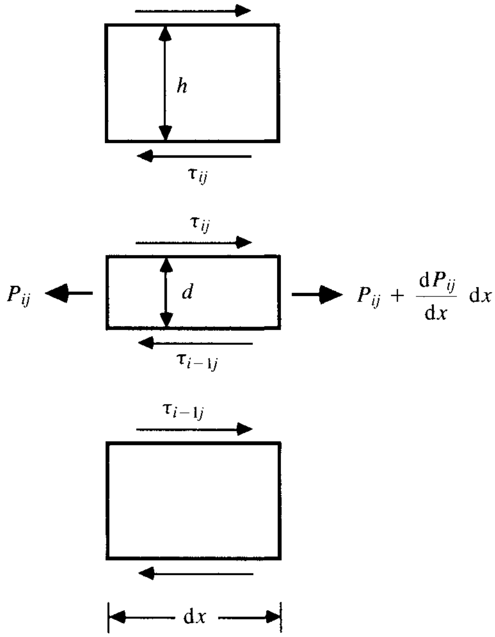

fibers. Given i (=1 and 2) and j (=1 and 2) as shown in Fig. 4.4, the following general solutions of u_{ij} and P_{ij} are obtained from Eqs. (4.4) and (4.5):

$$
\begin{aligned}
u_{11} &= A_1 + B_1\xi + C_1 e^{\lambda_1 \xi} + D_1 e^{-\lambda_1 \xi} \\
u_{21} &= A_1 + B_1\xi - \tfrac{1}{2}(C_1 e^{\lambda_1 \xi} + D_1 e^{-\lambda_1 \xi}) \\
P_{11} &= E_f\{B_1 + \lambda_1(C_1 e^{\lambda_1 \xi} - D_1 e^{-\lambda_1 \xi})\} \\
P_{21} &= E_f\{B_1 - \tfrac{1}{2}\lambda_1(C_1 e^{\lambda_1 \xi} - D_1 e^{\lambda_1 \xi})\} \\
u_{12} &= A_2 + B_2\xi + C_2 e^{\lambda_2 \xi} + D_2 e^{-\lambda_2 \xi} \\
u_{22} &= A_2 + B_2\xi - \frac{k}{2}(C_2 e^{\lambda_2 \xi} + D_2 e^{-\lambda_2 \xi}) \\
P_{12} &= E_m\{B_2 + \lambda_2(C_2 e^{\lambda_2 \xi} - D_2 e^{-\lambda_2 \xi})\} \\
P_{22} &= E_f\left\{B_2 - \frac{k}{2}\lambda_2(C_2 e^{\lambda_2 \xi} - D_2 e^{-\lambda_2 \xi})\right\}
\end{aligned}
\tag{4.6}
$$

where

$$
\begin{aligned}
&\xi = x/d, \quad \alpha_{ij} = E_{ij}h/Gd \\
&k = E_m/E_f \\
&\lambda_j = \sqrt{\left(\frac{\alpha_{1j} + 2\alpha_{2j}}{\alpha_{1j}\alpha_{2j}}\right)}
\end{aligned}
$$

and A_1, B_1, C_1, D_1, A_2, B_2, C_2 and D_2 are unknown constants.

The axial force and boundary conditions of the model of Fig. 4.4 are

(i) *symmetry conditions*

$$
(u_{11})_{\xi=0} = 0, \quad (u_{21})_{\xi=0} = 0, \quad (u_{12})_{\xi=\xi_1} = (u_{22})_{\xi=\xi_1} \tag{4.7}
$$

Fig. 4.4. An example of a three-row fiber model. (After Fukuda and Chou 1981a.)

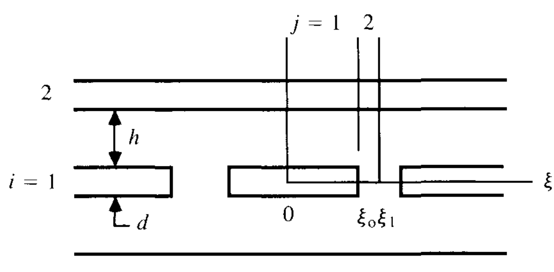

(ii) *continuity conditions*

$$(u_{11})_{\xi=\xi_o} = (u_{12})_{\xi=\xi_o}, \ (u_{21})_{\xi=\xi_o} = (u_{22})_{\xi=\xi_o}$$
$$(P_{11})_{\xi=\xi_o} = (P_{12})_{\xi=\xi_o}, \ (P_{21})_{\xi=\xi_o} = (P_{22})_{\xi=\xi_o} \tag{4.8}$$

(ii) *equilibrium of force*

$$P_{11} + 2P_{21} = 3P_o, \qquad P_{12} + 2P_{22} = 3P_o \tag{4.9}$$

where $3P_o$ denotes the total applied load, and ξ_o and ξ_1 are given in Fig. 4.4. The above conditions provide nine equations, of which eight are independent, to determine the eight integral constants of Eqs. (4.6). Finally, the axial load distribution becomes:

$$P_{11}/P_o = 1 - \frac{2\lambda_1(1-k)}{3F} \sinh \lambda_2(\xi_1 - \xi_o) \cosh \lambda_1 \xi$$

$$P_{21}/P_o = 1 + \frac{\lambda_1(1-k)}{3F} \sinh \lambda_2(\xi_1 - \xi_o) \cosh \lambda_1 \xi$$

$$P_{12}/P_o = \frac{3k}{2+k}\left\{1 + \frac{2\lambda_2(1-k)}{3F} \sinh \lambda_1 \xi_o \cosh \lambda_2(\xi - \xi_1)\right\} \tag{4.10}$$

$$P_{22}/P_o = \frac{3}{2+k}\left\{1 - \frac{k\lambda_2(1-k)}{3F} \sinh \lambda_1 \xi_o \cosh \lambda_2(\xi - \xi_1)\right\}$$

where

$$F = k\lambda_2 \cosh \lambda_2(\xi_1 - \xi_o) \sinh \lambda_1 \xi_o + \frac{2+k}{3} \lambda_1 \sinh \lambda_2(\xi_1 - \xi_o) \cosh \lambda_1 \xi_o$$

The displacement field can also be obtained with the given boundary conditions.

Limiting cases such as a single short fiber, a semi-infinite fiber and two semi-infinite fibers separated by a gap can be deduced from Fig. 4.4. Furthermore, the solution for the case where no load is transferred at fiber ends can be obtained by setting $k = 0$ in Eqs. (4.10). Figure 4.5 shows the axial load distributions, for several E_f/E_m values, in the continuous and discontinuous fibers. Fukuda and Chou (1981a) also concluded that the axial load distributions near the fiber ends are essentially the same for fibers of different length for given h/d and E_f/E_m values. This is demonstrated in Fig. 4.6 for the fiber configuration of Fig. 4.4. This finding is consistent with Rosen's (1964) definition of ineffective length (Section 3.4.6.1) which is independent of the actual fiber length (Chen 1971; Fukuda and Kawata 1977). Fukuda and Chou (1981b) have also considered the effects of load transfer at fiber ends and plastic deformation in the matrix.

4.3 Elastic properties

The elastic behavior of short-fiber composites has been extensively studied. It is convenient to subdivide short-fiber composites into three categories, according to their fiber orientations,

Fig. 4.5. Effect of E_f/E_m on fiber axial load distribution, for $h/d = 1$, $\xi_o/d = 100$, $\xi_1/d = 120$. ξ_o and ξ_1 are defined in Fig. 4.4. (a) Continuous fiber, and (b) discontinuous fiber. (After Fukuda and Chou 1981a.)

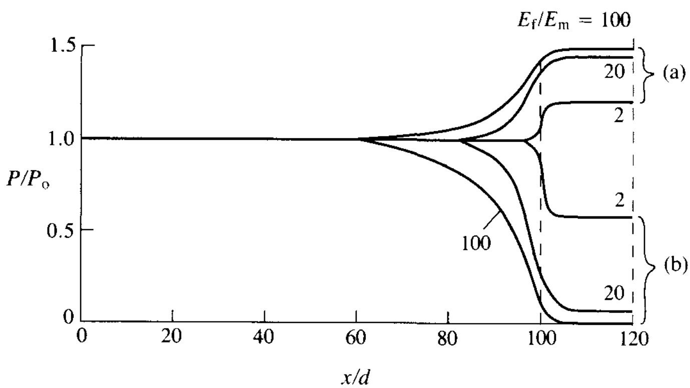

Fig. 4.6. Axial load distribution for fiber 1, and definition of fiber ineffective length. $h/d = 1$, $E_f/E_m = 20$, and δ = ineffective length. (After Fukuda and Chou 1981a.)

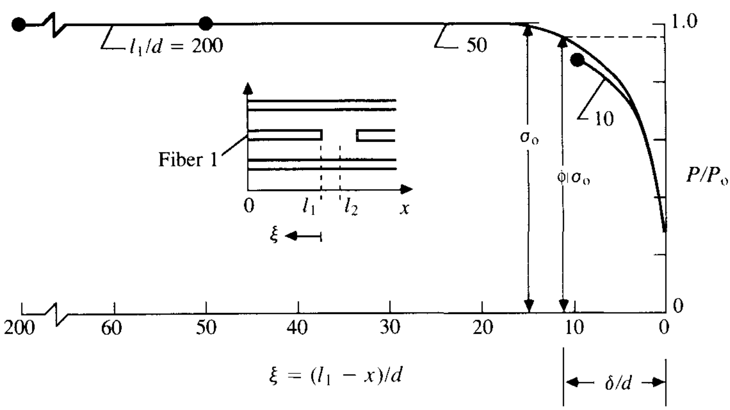

for the purpose of stiffness discussions: (1) unidirectionally aligned short fibers, (2) partially aligned short fibers, and (3) random short fibers.

4.3.1 *Unidirectionally aligned short-fiber composites*

For unidirectionally aligned short-fiber composites, the focus is on the effect of fiber length. Two major approaches are presented for the prediction of elastic moduli of aligned short-fiber composites. The first one is based upon a self-consistent model and the second one gives the upper and lower bounds of elastic moduli. The validity of some semi-empirical and numerical solutions is also examined.

4.3.1.1 *Shear-lag analysis*

Using Cox's fiber stress expression of Eqs. (4.3), the average fiber stress is

$$\begin{aligned}\bar{\sigma}_{\mathrm{f}} &= \frac{1}{l}\int_0^l \sigma_{\mathrm{f}}\,\mathrm{d}x \\ &= E_{\mathrm{f}}\varepsilon\left(1-\frac{\tanh(\beta l/2)}{\beta l/2}\right)\end{aligned} \tag{4.11}$$

Based upon Eq. (4.11), the effective axial Young's modulus of the short-fiber composite is approximated by

$$E_{11} = E_{\mathrm{f}} V_{\mathrm{f}} f(l) + E_{\mathrm{m}}(1-V_{\mathrm{f}}) \tag{4.12}$$

where

$$f(l) = 1-\frac{\tanh(\beta l/2)}{\beta l/2} \tag{4.13}$$

and it represents a reduction of the composite elastic modulus due to the finite length of the fiber.

4.3.1.2 *Self-consistent method*

The self-consistent method is a rigorous approach based upon the assumptions that the fiber and matrix materials are isotropic, homogeneous and linearly elastic, the fiber–matrix interfacial bonding is perfect, and the composite with aligned fibers is macroscopically homogeneous and transversely isotropic. As reviewed by Chamis and Sendeckyj (1968), there exist two basic variants of the self-consistent approach, namely the method by Hill (1965a&b) and that used by Kilchinskii (1965, 1966) and Hermans

(1967). Hill followed the method proposed by Kröner (1958) for aggregates of crystals and modeled the composite as a single long fiber embedded in an unbounded homogeneous medium which is macroscopically indistinguishable from the composite. The model of Kilchinskii and Hermans, on the other hand, consists of three concentric cylinders: the innermost cylinder has the elastic properties of the fiber, the middle one simulates the pure matrix material, and the outer one is unbounded and has the properties of the composite. Hill has shown that the prediction of the self-consistent method is more reliable at low and intermediate fiber contents.

The approach of Hill has been adopted by Chou, Nomura and Taya (1980) to treat the stiffness of short-fiber composites. In their work, a single inclusion is assumed to be embedded in a continuous and homogeneous medium (see Hill 1952; Eshelby 1957; Hashin and Rosen 1964; Mura 1982). The inclusion has the elastic properties of a short fiber while the surrounding material possesses the properties of the composite. It is the unknown elastic property of the composite that needs to be found. The work of Chou *et al.* does not restrict the number of component phases in the composite and is hence applicable to hybrid composites (Chapter 5). Numerical examples of this self-consistent approach are given for the special case of a binary system of one kind of fiber in a matrix. Figure 4.7 shows the variation of longitudinal modulus E_{11} of a glass/epoxy system with inclusion volume fraction V_f at three different inclusion aspect ratios (l/d). For $l/d = 100$ the self-consistent theory predicts that the inclusions behave like continuous fibers and the rule-of-mixtures is valid. Also shown in Fig. 4.7 are the predictions of the semi-empirical relation of Halpin and Tsai (see Halpin 1984). The discrepancy between the self-consistent theory and the Halpin–Tsai equation is most pronounced at intermediate values of the aspect ratio. Comparisons of the self-consistent approach with experiments are given in Section 4.3.2, where the effect of fiber misorientation is taken into account.

The predictions of elastic stiffness for particulate-filled composites have been performed by a number of investigators, including Kerner (1956), van der Poel (1958), Hashin and Shtrikman (1963) and Budiansky (1965). The self-consistent theory reduces to Budiansky's solution for the special case of $l/d = 1$.

4.3.1.3 *Bound approach*

Nomura and Chou (1984) also adopted an alternate approach to short-fiber composite effective moduli by deriving their upper and lower bounds. This approach was motivated by the work of Eshekby (1961), Hashin (1965a), Kröner (1967, 1972, 1977), Dederichs and Zeller (1973), Zeller and Dederichs (1973), Wu and McCullough (1977), and Christensen (1979). Nomura and Chou adopted a perturbation expansion of the composite local strain based upon the elastic Green's function. The effective elastic constants can be expressed in infinite series form. When the series are written in terms of the stiffness constants, the first term is the well known Voigt average (1889). The first term of the series represents the Reuss average (1929) when the expression is written in terms of the compliance constants. Based upon the assumptions that the short fibers are modeled as aligned ellipsoidal inclusions and distributed in the matrix material in a statistically homogeneous manner, Nomura and Chou have evaluated the series expressions of the elastic constants up to the third-order term. A variational treatment has been utilized to derive the bounds of the effective elastic moduli of the unidirectional short-fiber composite.

Fig. 4.7. The variation of E_{11}/E_m with V_f at various l/d values for $E_f/E_m = 20$, $\nu_f = 0.3$ and $\nu_m = 0.35$. —— self-consistent approach; - - - - Halpin–Tsai equation. (After Chou, Nomura and Taya 1980).

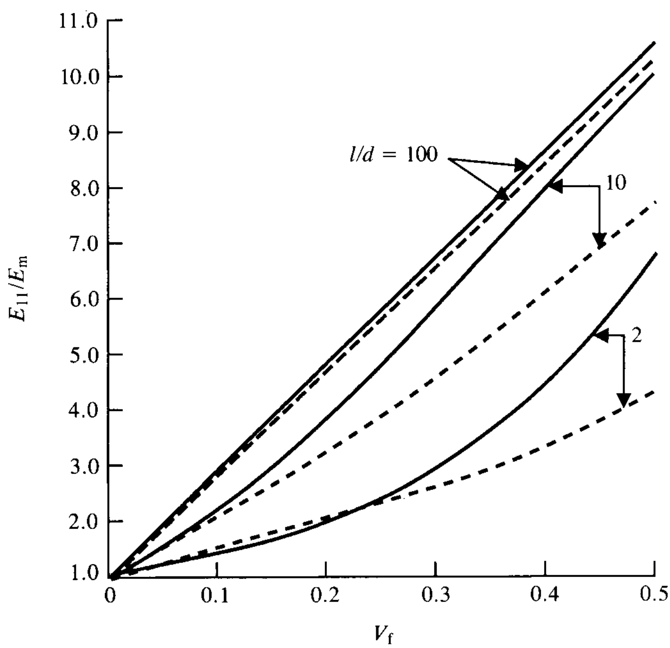

Figure 4.8 illustrates the variation of the axial Young's modulus E_{11} (normalized by the matrix modulus E_m) with fiber volume fraction V_f at fiber aspect ratios $l/d = 1$, 5 and ∞, for glass/epoxy composites. The solid lines indicate the upper and lower bound predictions; the predictions of the self-consistent model of Chou, Nomura and Taya (1980) are indicated by broken lines. The self-consistent model prediction is close to the lower bound at low fiber volume fraction and approaches the upper bound at high fiber volume fraction. The gap between the bounds at a fixed fiber volume fraction narrows as the fiber aspect ratio increases. For long continuous fibers, the bound approach and the self-consistent model all predict the rule-of-mixtures relation. Although fiber volume fraction in the full range of 0 to 1 is used in Fig. 4.8, it is understood that the maximum attainable fiber volume fraction in a composite is determined by the fiber geometric packing and fiber cross-sectional shape.

Figure 4.9 shows the comparison of the bound approach with Hashin's (1965a) results for the effective axial shear modulus G_{12} of continuous fiber composites. The theory of Nomura and Chou (1984) predicts tighter bounds than those of Hashin. This is due to

Fig. 4.8. The variation of E_{11}/E_m with V_f for $E_f/E_m = 20$, $\nu_m = 0.4$ and $\nu_f = 0.3$ —— bound approach; - - - - self-consistent model. (After Nomura and Chou 1984).

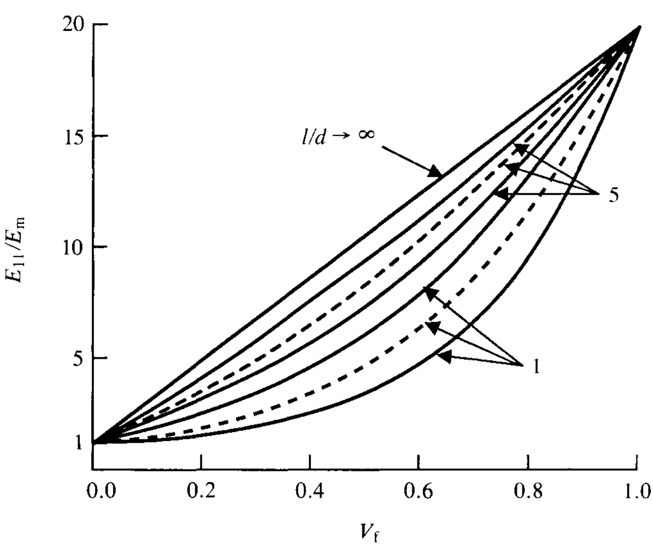

the fact that Hashin's result is equivalent to the evaluation of the series expression of the elastic constants up to the second-order term. The bounds of effective elastic moduli of multi-phase systems such as hybrid composites can also be examined by this approach.

4.3.1.4 *Halpin–Tsai equation*

The Halpin–Tsai equation (see Halpin 1984) was obtained by reducing Hermans' solution (1967) to a simpler analytical form while the filament geometries are taken into account through the use of some empirical factors. The pertinent relations are

$$\frac{\bar{P}}{P_m} = \frac{1 + \zeta\eta V_f}{1 - \eta V_f}$$
$$\nu_{12} \cong \nu_f V_f + \nu_m V_m \tag{4.14}$$

Fig. 4.9. The variation of G_{12}/G_m with V_f for $E_f/E_m = 20$, $\nu_m = 0.4$, $\nu_f = 0.3$ and $l/d \to \infty$. —— bound approach; – – – – self-consistent model; —·—·— bounds of Hashin and Shtrikman. (After Nomura and Chou 1984).

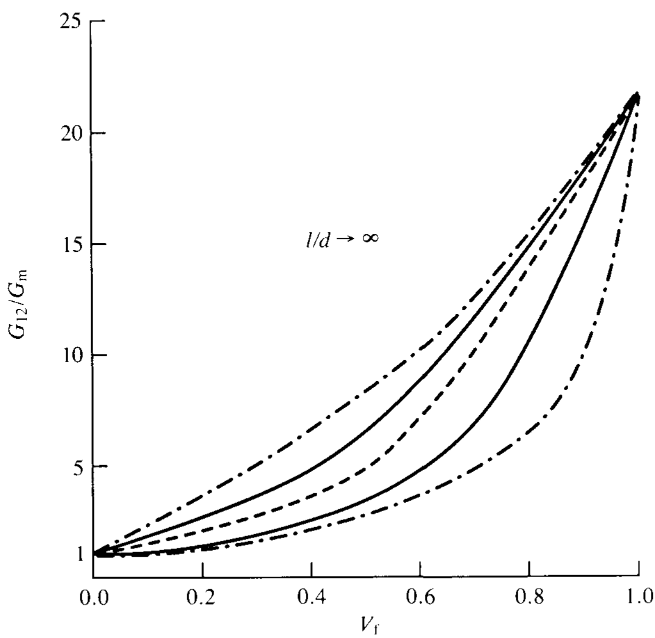

where

$$\eta = (P_f/P_m - 1)(P_f/P_m + \zeta)$$

$$\zeta(E_{11}) = 2\left(\frac{l}{d}\right) + 40V_f^{10}$$

$$\zeta(E_{22}) = 2 + 40V_f^{10}$$

$$\zeta(G_{12}) = 1 + 40V_f^{10}$$

$$\zeta(G_{23}) \cong 1/(4 - 3\nu_m)$$

$$\bar{P} = E_{11},\ E_{22},\ G_{12} \text{ or } G_{23}$$

$$P_f = E_f \text{ (for } E_{11} \text{ and } E_{22}\text{) or } G_f \text{ (for } G_{12} \text{ and } G_{23}\text{)}$$

$$P_m = E_m \text{ (for } E_{11} \text{ and } E_{22}\text{) or } G_m \text{ (for } G_{12} \text{ and } G_{23}\text{)}$$

Other solutions of effective elastic constants can be found from, for instance, the numerical work of Conway and Chang (1971), and Chang, Conway and Weaver (1972). Experimental data on short-fiber composite elastic properties have been reported by Lees (1968), and Blumentritt, Vu and Cooper (1974).

4.3.2 *Partially aligned short-fiber composites*

It is usually desirable to orient the fibers for enhanced stiffness and strength properties. However, perfect alignment of short fibers in a composite is normally very difficult to achieve. Partial fiber alignment is typical in, for example, injection molded composites. Several different approaches have been adopted by researchers to predict the stiffness of short-fiber composites with biassed fiber orientation. The following discussions of these approaches begin with a brief summary of the original treatments on misaligned continuous fibers.

The first attempt in examining the effect of fiber orientation is attributed to the work of Cox (1952), who studied the elastic properties of paper and other fibrous materials. Cox's model is concerned with continuous fibers of negligible thickness with orientations either random or defined by some distribution rules. The contribution of matrix to stiffness is ignored. It is also assumed in this model that under load the fibers do not slide across each other at the points of intersection (see Cook 1968).

Cook (1968) provides the elastic properties of continuous fiber composites in three dimensions. The systems of misorientation examined by Cook include the axially symmetric type, a fan shaped array and systems of crossed fibers. Fiber orientation distribution functions are generated analytically to describe the characteristics of these systems. A case of most practical significance is the axially symmetric fiber distribution, which is also termed the *witch's broom* by Cook. The degree of fiber scatter from perfect alignment is described by the root-mean-square deviation of orientation from the symmetry axis

$$s^2 = \int_0^{\pi/2} \eta(\theta)\theta^2 \sin\theta \, d\theta \tag{4.15}$$

where $\eta(\theta)$ is the fiber orientation distribution function. According to Cook, for a composite such as glass fibers in a polymer resin ($V_f E_f / V_m E_m \sim 20$) the orientation effect can be minimized if the fibers are sufficiently long and, hence, a high degree of orientation can be achieved. On the other hand, for whisker reinforced composites the reduction in stiffness may be significant if the fibers are short and alignment becomes a difficult technical problem. Cook reported that for a silicon nitride whisker reinforced epoxy resin composite examined, stiffness reduction of 4–19% could occur for the root-mean-square scatter between 4.5° and 10°.

Fukuda and Kawata (1974) considered the Young's modulus of short-fiber composites and took into consideration variations in both fiber length and orientation. The analysis is based upon the plane stress elasticity solution of load transfer between the fiber and matrix in a single short-fiber model, and the assumption of negligible interactions between neighboring fibers. The prediction of the composite Young's modulus is given in the general form

$$E_c = C_l C_\theta E_f V_f + E_m(1 - V_f) \tag{4.16}$$

The factors C_l and C_θ reflect the effects of fiber length and orientation distributions, respectively. Both C_l and C_θ are unity in the case of aligned continuous fibers.

Figure 4.10 shows the variations of C_l with the factor $(l/d)(E_f/E_m)$ where l/d denotes the fiber aspect ratio. The open and solid circles in Fig. 4.10 are experimental values of Anderson and Lavengood (1968) for glass/epoxy and boron/epoxy, respectively. The solid line is obtained from a two-dimensional analysis and the broken line is the modified result when the fiber circular cross-sectional shape is taken into account. Figure 4.11 shows the variations of C_θ with $\eta(\theta)$, which is the probability density of fibers at the orientation angle θ. Fukuda and Kawata assume that $\int_0^{\pi/2} \eta(\theta)\, d\theta = 1$. Three forms of $\eta(\theta)$ are assumed: rectangular, sinusoidal and triangular. θ_o defines the range of fiber angular distribution. Comparisons of the predictions of Eq. (4.16) with the measured modulus of an α-SiC whisker/aluminum composite (Schierding and Deex 1969) are favorable.

The above discussions have centered upon either continuous fibers or short fibers in planar arrangement. A treatment of the three-dimensional fiber orientation effect has been developed by Chou and Nomura (1981). They considered an axially symmetrical fiber orientation distribution. Referring to Fig. 4.12, the general orientation of a short fiber can be considered as derived from the

Fig. 4.10. Relation between C_l and $(l/d)/(E_f/E_m)$. (After Fukuda and Kawata 1974).

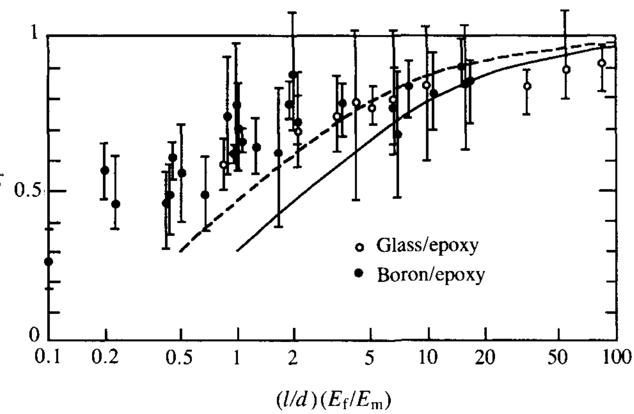

Fig. 4.11. Relation between C_θ and θ_o. (After Fukuda and Kawata 1974).

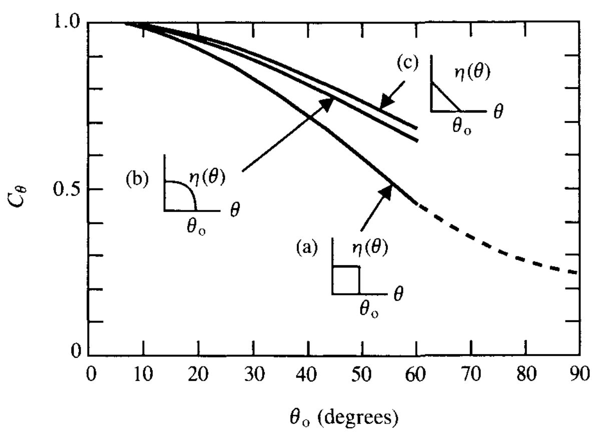

original position along the z axis by two rotations. The corresponding rotational angles are φ and θ, as indicated in Fig. 4.12. The transformation matrix, from the original coordinate system to the current system, is defined as

$$[T] = \begin{bmatrix} \sin\theta\cos\varphi & \sin\theta\sin\varphi & \cos\theta \\ \cos\theta\cos\varphi & \cos\theta\sin\varphi & -\sin\theta \\ -\sin\varphi & \cos\varphi & 0 \end{bmatrix} \tag{4.17}$$

Let the bold-faced letter indicate a tensor. The transformation of an elastic stiffness tensor **C** (or compliance tensor **S**) of a unidirectionally aligned short-fiber composite can be performed through the application of the **T** matrix and the resulting tensor is denoted by $\mathbf{C}'$ (or $\mathbf{S}'$). The effective elastic tensor of a misaligned short-fiber composite is then given by

$$\begin{aligned} \mathbf{C}'' &= \int \mathbf{C}'(\theta, \varphi)\eta(\theta, \varphi)\,\mathrm{d}A \\ &= \int_0^{2\pi} \mathrm{d}\varphi \int_0^{\pi} \mathbf{C}'(\theta, \varphi)\eta(\theta, \varphi)\sin\theta\,\mathrm{d}\theta \end{aligned} \tag{4.18}$$

Here, $\eta(\theta, \varphi)$ in the above equation is the probability density function of fiber orientation determined from experiments. The integration is carried out over the surface area of a unit sphere to include all the fibers in the composite.

Fig. 4.12. Reference coordinate axes.

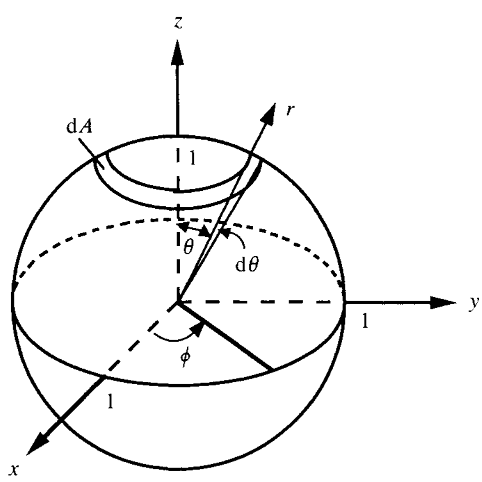

Two cases of fiber orientation distribution are of practical importance. In the case of injection molded objects, fiber orientation distribution is independent of the angle φ if the direction of flow is along the z axis, and $\eta = \eta(\theta)$. The composite in this case is isotropic in the plane transverse to the z axis, and $\mathbf{C}''$ is independent of φ. In sheet molding compounds, it is reasonable to assume that the short fibers all lie on the xz plane and the problem is two-dimensional. The transformation matrix is

$$T = \begin{bmatrix} \sin\theta & 0 & \cos\theta \\ \cos\theta & 0 & -\sin\theta \\ 0 & 1 & 0 \end{bmatrix} \tag{4.19}$$

Equation (4.18) is then reduced to

$$\mathbf{C}'' = 2\pi \int_0^{\pi} \mathbf{C}'(\theta)\eta(\theta)\sin\theta\,\mathrm{d}\theta \tag{4.20}$$

It has been pointed out in the variational treatment of Section 4.3.1 that the first term in the series expression of composite stiffness constant or compliance constant gives the well known Voigt's upper bound or Reuss' lower bound. The averaging principles of Voigt and Reuss were first used to predict the elastic properties of a polycrystalline aggregate in terms of the basic properties of a single crystal and its orientation in the aggregate. The Voigt and Reuss averages are equivalent to assuming that the single crystals are arrayed in parallel and in series, respectively. These concepts of Voigt and Reuss averages are also useful in dealing with misaligned composites. They can be expressed in the general forms for the stiffness constant $\mathbf{C}$ and compliance constant $\mathbf{S}$ as

$$\begin{aligned} \langle C \rangle &= \int_V \mathbf{C}(r, \theta, \varphi)\,\mathrm{d}V \Big/ \int_V \mathrm{d}V \\ \langle S \rangle &= \int_V \mathbf{S}(r, \theta, \varphi)\,\mathrm{d}V \Big/ \int_V \mathrm{d}V \end{aligned} \tag{4.21}$$

where, in general, $\mathbf{C}$ and $\mathbf{S}$ are functions of position (r, θ, φ) as shown in Fig. 4.12. Furthermore, it can be shown that in the Voigt and Reuss averaging processes for small fiber misalignment there is negligible difference between the model involving a distribution of fiber orientations and the model in which all the fibers are aligned along the direction of the root-mean-square average angle (see

Knibbs and Morris 1974). The treatment of effective elastic moduli for partially aligned short-fiber composites can also be achieved through the laminated plate analogue, which is discussed in Section 4.3.3.

4.3.3 *Random short-fiber composites*

The treatment of Cox (1952) discussed in Section 4.3.2 deals with the stiffness of *continuous* fibers distributed in a plane. For completely random fiber distribution, Cox's results are reduced to the simple forms

$$E_c = E_f V_f / 3$$
$$G_c = E_f V_f / 8 \tag{4.22}$$
$$\nu_c = \tfrac{1}{3}$$

where E_c, G_c and ν_c are, respectively, the Young's modulus, shear modulus and Poisson's ratio of the composite. The random distribution of fibers imparts isotropic properties of the composite at the macroscopic scale. Hence, E_c, G_c and ν_c satisfy the relationship for isotropic materials:

$$G_c = E_c / 2(1 + \nu_c) \tag{4.23}$$

The contribution of matrix material is neglected in this treatment but has been taken into account in the works of Arridge (1963), and Pakdemirli and Williams (1969), who also derived approximate expressions for E_c and G_c.

Nielsen and Chen (1968) proposed that the in-plane Young's modulus of a random composite with *continuous* fibers can be approximated by an averaging process. Basic to this process is the knowledge of the elastic moduli of a unidirectional fiber composite measured at an angle θ from the fiber direction (see Eqs. 2.19). The effective in-plane Young's modulus of a random composite, for example, is then given by

$$E_c = \frac{2}{\pi} \int_0^{\pi/2} E(\theta)\, d\theta \tag{4.24}$$

In applying Eq. (4.24), the fiber volume fraction of the composite used for calculating $E(\theta)$ should be the same as that in the random composite. It should also be noted that $E(\theta)$ is not a component of a tensor. Hence, the averaging process defined in Eq. (4.24) bears no relation to the Voigt and Reuss averages discussed in Section 4.3.2.

The elastic moduli of a composite where the short fibers exhibit in-plane random orientation can also be examined by the method of a laminate analogue (Halpin 1969; Halpin and Pagano 1969; Halpin, Jerine and Whitney 1971). The following discussions are based upon reviews by Kardos (1973) and Nicolais (1975). In the laminate analogue the mechanical response of the composite is simulated by that of a laminate composed of unidirectional short fibers (Kardos 1973). The laminate is symmetric about the mid-

Fig. 4.13. (a) Laminate analogue of a composite with random in-plane orientation of short fibers. The quasi-isotropic laminate has the $[+45°/-45°/90°/0°]_s$ configuration. (b) Dependence of tensile modulus on volume fraction of 3.2 mm E-glass/polycarbonate composites for random in-plane (dashed curve) and biassed (solid curves) fiber orientations. – – – – is quasi-isotropic calculation; —— weighted distribution calculations; ○, ● experimental data. Fiber aspect ratio is about 313. (After Halpin, Jerine and Whitney 1971).

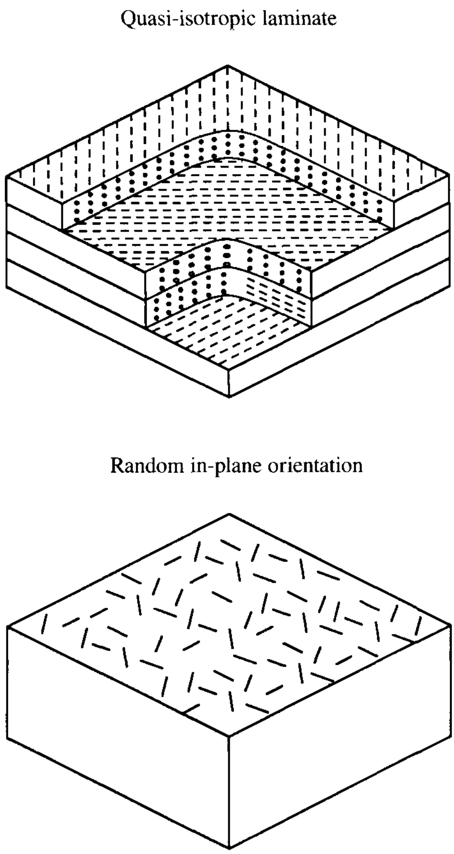

(a)

plane and has the same number of $+\theta$ and $-\theta$ orientation plies (Fig. 4.13a).

The concept of the laminate analogue is outlined in the following. First, the four independent elastic moduli E_{11}, E_{22}, ν_{12} and G_{12} of a unidirectional short-fiber lamina can be derived from the fiber and matrix properties based upon the self-consistent model, the variational method, or the Halpin–Tsai equation. The stiffness matrix components Q_{ij} are given by Eqs. (2.14). The effective engineering stiffness constants E_{11} E_{22}, ν_{21} and G_{12} for the aligned short-fiber lamina can be expressed in terms of the Q_{ij}'s as given in Table 2.1.

The stiffness matrix components $\bar{Q}_{ij}$ for a unidirectional lamina oriented at an angle θ with respect to the x axis are given in Eqs. (2.16). They can also be written in the following alternate forms:

$$\begin{aligned}
\bar{Q}_{11} &= U_1 + U_2 \cos 2\theta + U_3 \cos 4\theta \\
\bar{Q}_{22} &= U_1 - U_2 \cos 2\theta + U_3 \cos 4\theta \\
\bar{Q}_{12} &= U_4 - U_3 \cos 4\theta \\
\bar{Q}_{66} &= U_5 - U_3 \cos 4\theta \\
\bar{Q}_{16} &= \tfrac{1}{2} U_1 \sin 2\theta + U_3 \sin 4\theta \\
\bar{Q}_{26} &= \tfrac{1}{2} U_2 \sin 2\theta - U_3 \sin 4\theta
\end{aligned} \tag{4.25}$$

Fig. 4.13. (*cont.*).

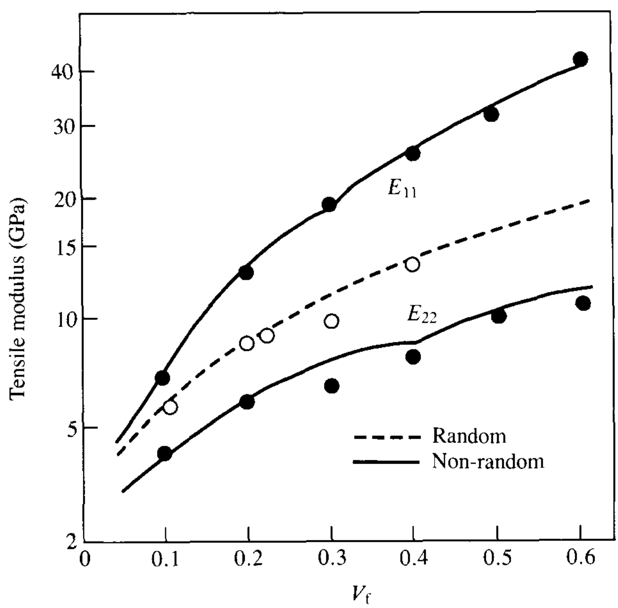

(b)

where the U_i are defined as

$$U_1 = \tfrac{1}{8}(3Q_{11} + 3Q_{22} + 2Q_{12} + 4Q_{66})$$
$$U_2 = \tfrac{1}{2}(Q_{11} - Q_{22})$$
$$U_3 = \tfrac{1}{8}(Q_{11} + Q_{22} - 2Q_{12} - 4Q_{66})$$
$$U_4 = \tfrac{1}{8}(Q_{11} + Q_{22} + 6Q_{12} - 4Q_{66})$$
$$U_5 = \tfrac{1}{8}(Q_{11} + Q_{22} - 2Q_{12} + 4Q_{66})$$

When the plies are stacked together to form a laminate, the in-plane stretching stiffness A_{ij} is given by Eqs. (2.29). For the case of a balanced angle-ply ($\pm\theta$) composite with mid-plane symmetry, the bending stiffness B_{ij} (Eqs. 2.29) and the coupling terms A_{16} and A_{26} vanish, and the A_{ij} components can be represented by

$$\begin{aligned} A_{11} &= [U_1 + U_2\cos 2\theta + U_3\cos 4\theta]h \\ A_{22} &= [U_1 - U_2\cos 2\theta + U_3\cos 4\theta]h \\ A_{12} &= [U_4 - U_3\cos 4\theta]h \\ A_{66} &= [U_5 - U_3\cos 4\theta]h \end{aligned} \tag{4.26}$$

Here, h denotes the total laminate thickness. Following the same reasoning for the derivation of Eq. (2.15), the effective engineering constants of the laminate are given by

$$\begin{aligned} E_{11} &= \frac{A_{11}A_{22} - A_{12}^2}{A_{22}\cdot h} \\ E_{22} &= \frac{A_{11}A_{22} - A_{12}^2}{A_{11}\cdot h} \\ \nu_{12} &= \frac{A_{12}}{A_{22}} \\ G_{12} &= \frac{A_{66}}{h} \end{aligned} \tag{4.27}$$

If a random short-fiber composite assumes the form of a thin sheet while the sheet thickness is less than the average fiber length, the composite can be modeled as a 'quasi-isotropic laminate'. In principle, the laminate can be constructed by stacking up unidirectional laminae in all orientations to achieve a balanced and symmetric arrangement. Because the fiber orientation covers all the values between 0° and 180°, the angular dependent terms in the A_{ij}

components of Eqs. (2.16) cancel one another. Consequently, the effective engineering constants can be simplified as

$$E_c = 4U_5 \frac{U_1 - U_5}{U_1}$$

$$\nu_c = \frac{U_1 - 2U_5}{U_1} \tag{4.28}$$

$$G_c = U_5$$

It is obvious that the above elastic constants satisfy the necessary relation for in-plane isotropy. Expressions for random fiber composite elastic constants equivalent to Eqs. (4.28) also have been obtained by Akasaka (1974). Halpin, Jerine and Whitney (1971) have demonstrated the validity of the laminate analogue by comparing the analytical predictions with the measurement of effective tensile modulus of E-glass/polycarbonate with random fiber orientation as shown in Fig. 4.13(b).

The laminate analogue can also be applied to quasi-isotropic short-fiber composites using lay-ups such as 0°/±60° and 0°/±45°/90° (Warren and Norris 1953). Other works dealing with the elastic stiffness of random fiber composites can be found from Tsai and Pagano (1968); Manera (1971); Christensen and Waals (1972); Wilczynki (1978); and Hahn (1978). As pointed out by Bert (1979), the accuracy of these approximations is affected by the fiber volume fraction and the ratio E_f/E_m. The laminate analogue can also be used for examining the elastic properties of short-fiber composites with layered microstructures. Figure 4.14 shows the scanning electron micrograph of the cross-section of an injection molded polyethylene terephthalate with short glass fibers. This type of layered structure has been found in many types of short-fiber reinforced thermoplastics.

Attempts also have been made to predict the stiffness of composites with random fibers in three-dimensional distribution. Rosen and Shu (1971) and Christensen and Waals (1972) examined the case of continuous fibers. Halpin, Jerine and Whitney (1971) treated the case of layers of plain woven fabric in which the unit weave cell is pierced by a straight yarn perpendicular to the fabric plane. The problem of random short fiber orientation in three dimensions has been treated by Chou and Nomura (1981). By taking $\eta = 1/2\pi$ in Eq. (4.18), elastic moduli for completely random orientation can be obtained. Figure 4.15 illustrates the theoretical variations of E_c/E_m with V_f for a random glass/epoxy system and the experimental data of Manera (1971).

The laminated plate analogue developed above can also be applied to consider in-plane partially aligned short fibers (Halpin, Jerine and Whitney 1971; Kardos 1973) discussed in Section 4.3.2. In this case the angular fiber distribution function $\eta(\theta)$ needs to be measured from the composite specimen. The laminate simulating the composite is treated as composed of weighted groups of angle plies ($\pm\theta$) with fixed fiber volume fraction. The percentage of materials oriented at the angles $\pm\theta$ is obtained from $\eta(\theta)$. The contributions to the overall response of laminate stiffness from different layers are proportioned to their fractional thickness in the laminate.

Table 4.1 gives an example of the orientation distributions of discontinuous glass fibers in a polymeric matrix. The composite is

Fig. 4.14. SEM micrograph of short glass fiber/polyethylene terephthalate showing layered structure of fiber orientations. (After Friedrich and Karger-Kocsis 1989.)

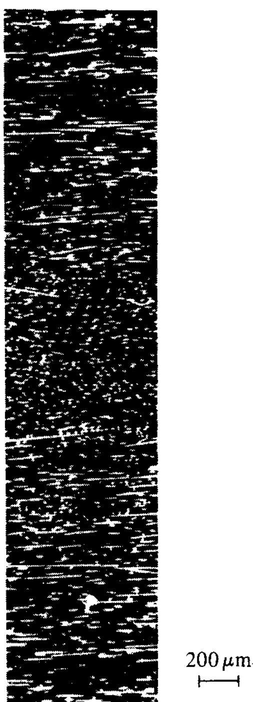

compression molded from extrudate. It can be seen that most of the fibers are oriented quite close to the extrusion direction. Whereas previously each $\pm\theta$ ply was weighted equally in summing up the stiffness contributions to the laminate, one must now account for the fact that more of the laminate thickness may be made up of one angle than the other. Define $a(\theta)/h$ as the percentage of the material oriented at the angles $\pm\theta$, and it is obtained from the experimental angular distribution $\eta(\theta)$ where $\int_0^\pi \eta(\theta)\,d\theta = 1$. The stiffness moduli A_{ij} of the laminate is related to the stiffness of the plies $A_{ij}(\theta_k)$, oriented at the angles $\pm\theta_k$, by

$$A_{ij} = \sum_{k=1}^{n} \frac{a(\theta_k)}{h} A_{ij}(\theta_k) \tag{4.29}$$

where n is the total number of plies.

In summary, the calculation of the effective engineering stiffness of short-fiber composites with biassed fiber orientations should first follow the procedure outlined in Section 2.3 to obtain the A_{ij} components for each fiber angle. These are then summed according to their fiber angular distributions such as that given in Table 4.1 and Eq. (4.29) to obtain the A_{ij} terms. The engineering constants are then obtained from Eqs. (4.27). The solid lines in Fig. 4.13(b)

Fig. 4.15. The comparison of E_c/E_m (—— bound approach; - - - - self-consistent model) with experimental data for $E_f/E_m = 32.4$, $\nu_m = 0.4$, $\nu_f = 0.25$ and $l/d \to \infty$. (After Chow and Nomura 1981.)

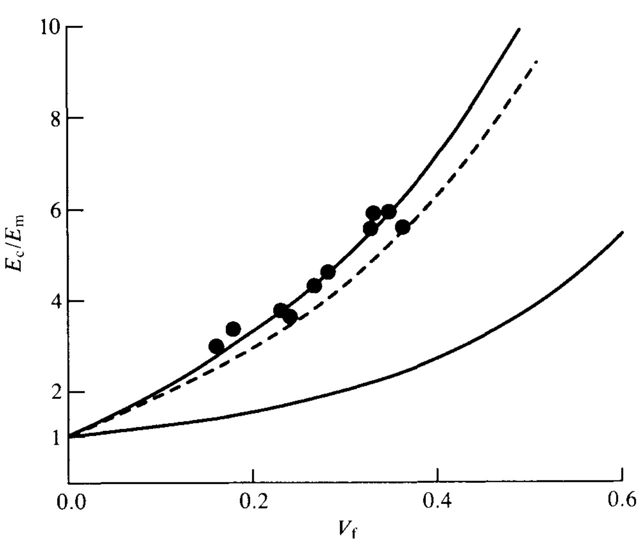

are theoretical predictions of the tensile moduli based upon this procedure. The bumps in the curves are attributed to the fact that the angular distribution functions are not smooth functions of fiber volume fraction.

4.4 Physical properties

The physical properties described below include thermal conductivity and thermal expansion coefficients. These properties are essential to the study of the thermomechanical behavior of short-fiber composites.

4.4.1 *Thermal conductivity*

The important transport properties of composites include dielectric constant, heat conduction, electrical conduction, magnetic

Table 4.1. *Fiber orientation distributions in composites compression molded from rod extrudate. Short glass fiber aspect ratio* ≈ 313. *After Halpin et al.* (1971)

Orientation θ (degrees)	Percent fibers having θ orientation			
2.5	23.4	25.4	25.0	36.5
7.5	17.9	18.1	23.8	23.9
12.5	12.0	12.3	16.4	14.2
17.5	16.0	7.7	10.0	5.7
22.5	6.2	6.4	6.8	3.0
27.5	5.9	5.6	4.8	2.7
32.5	4.4	4.6	3.1	1.8
37.5	4.6	3.1	2.4	2.0
42.5	2.6	3.4	1.6	1.0
47.5	1.7	1.9	1.3	0.4
52.5	0.4	1.3	0.8	0.7
57.5	0.7	0.7	1.1	0.8
62.5	1.0	1.4	0.9	0.5
67.5	0.7	1.1	0.7	0.7
72.5	0.1	2.1	0.4	0.5
77.5	0.9	0.9	0.6	0.8
82.5	0.5	2.3	0.3	0.9
87.5	1.0	1.4	0.1	0.8
Fiber volume fraction	20	30	40	50

permeability and diffusion coefficients. Since all these properties are second rank tensors, only the bounds of thermal conductivity are demonstrated.

The linear relation between the heat flux $\mathbf{q}$ and gradient of temperature T is given by

$$\mathbf{q} = \mathbf{k}(-\nabla T) \tag{4.30}$$

where $\mathbf{k}$ denotes thermal conductivity and is assumed to be a function of position only. It is understood that $\mathbf{k}$ is a symmetric tensor quantity. The governing equation for a steady-state heat conduction is

$$\nabla \cdot \mathbf{q} = 0 \tag{4.31}$$

Several approaches to this subject have been employed by researchers. These include the statistical method by Beran (1965), Beran and Molyneux (1966), and Hori and Yonezawa (1975) as well as the self-consistent and variational approaches of Hashin and Shtrikman (1962), Hashin (1968) and Willis (1977).

Nomura and Chou (1980), following their development of bounds of elastic moduli (1984), derived bounds of effective thermal conductivity of unidirectional short-fiber composites. The short fibers are again modeled as ellipsoidal inclusions of the same length and are distributed in a statistically homogeneous manner in the matrix material. The composite exhibits transverse isotropy. This approach is also valid for composites containing more than one type of fiber. Consider the case of a binary system and denote the thermal conductivity and volume fraction of the fiber and matrix phases by k_{f}, V_{f} and k_{m}, V_{m}, respectively. The bounds of the effective composite conductivity k_{11} along the fiber directions are

$$\left\{\frac{V_{\mathrm{f}}}{k_{\mathrm{f}}}+\frac{V_{\mathrm{m}}}{k_{\mathrm{m}}}-\frac{V_{\mathrm{f}}V_{\mathrm{m}}\left(\dfrac{1}{k_{\mathrm{f}}}-\dfrac{1}{k_{\mathrm{m}}}\right)^{2}h(t)}{(V_{\mathrm{m}}-V_{\mathrm{f}})\left(\dfrac{1}{k_{\mathrm{f}}}-\dfrac{1}{k_{\mathrm{m}}}\right)h(t)+\dfrac{V_{\mathrm{f}}}{k_{\mathrm{f}}}+\dfrac{V_{\mathrm{m}}}{k_{\mathrm{m}}}}\right\}^{-1} \leq k_{11}$$

$$\leq V_{\mathrm{f}}k_{\mathrm{f}}+V_{\mathrm{m}}k_{\mathrm{m}}-\frac{V_{\mathrm{f}}V_{\mathrm{m}}(k_{\mathrm{f}}-k_{\mathrm{m}})^{2}(1-h(t))}{(V_{\mathrm{m}}-V_{\mathrm{f}})(k_{\mathrm{f}}-k_{\mathrm{m}})(1-h(t))+V_{\mathrm{f}}k_{\mathrm{f}}+V_{\mathrm{m}}k_{\mathrm{m}}} \tag{4.32}$$

The bounds of the conductivity k_{22} and k_{33} in the transverse direction are

$$\left\{\frac{V_f}{k_f}+\frac{V_m}{k_m}-\frac{V_fV_m\left(\frac{1}{k_f}-\frac{1}{k_m}\right)^2(1-h(t)/2)}{(V_m-V_f)\left(\frac{1}{k_f}-\frac{1}{k_m}\right)(1-h(t)/2)+\frac{V_f}{k_f}+\frac{V_m}{k_m}}\right\}^{-1}\leq k_{22}=k_{33}$$

$$\leq V_fk_f+V_mk_m-\frac{V_fV_m(k_f-k_m)^2h(t)}{(V_m-V_f)(k_f-k_m)h(t)+2(V_fk_f+V_mk_m)} \quad (4.33)$$

where

$$h(t)=\frac{t^2}{t^2-1}\left\{1-\frac{1}{2}\left[\sqrt{\left(\frac{t^2}{t^2-1}\right)}\right.\right.$$
$$\left.\left.-\sqrt{\left(\frac{t^2-1}{t^2}\right)}\ln\left(\frac{t+\sqrt{(t^2-1)}}{t-\sqrt{(t^2-1)}}\right)\right]\right\} \quad (4.34)$$

and t denotes the aspect ratio l/d of the short fiber.

For the special case of spherical inclusions ($h(t)=\frac{2}{3}$), the composite is isotropic and Eqs. (4.32) and (4.33) are simplified as

$$\left[\frac{V_f}{k_f}+\frac{V_m}{k_m}-\frac{2V_fV_m\left(\frac{1}{k_f}-\frac{1}{k_m}\right)^2}{2(V_m-V_f)\left(\frac{1}{k_f}-\frac{1}{k_m}\right)+3\left(\frac{V_f}{k_f}+\frac{V_m}{k_m}\right)}\right]^{-1}\leq k\leq V_fk_f+V_mk_m$$
$$-\frac{V_fV_m(k_f-k_m)^2}{(V_f-V_m)(k_f-k_m)+3(V_fk_f+V_mk_m)} \quad (4.35)$$

In the case of continuous fibers, $h(t)=1$ and Eqs. (4.32) and (4.33) become

$$k_{11}=V_fk_f+V_mk_m \quad (4.36)$$

$$\frac{(k_m+k_f)k_mk_f}{(V_fk_m+V_mk_f)^2+k_mk_f}\leq k_{22}(=k_{33})\leq\frac{(V_mk_m+V_fk_f)^2+k_mk_f}{k_m+k_f} \quad (4.37)$$

Figure 4.16 illustrates the variations of k_{11}/k_m with fiber volume fraction of an E-glass/epoxy system for the limiting cases of $l/d\to\infty$ and $l/d=1$. The bounds of k_{11} converge to a single line for continuous fibers as indicated by Eq. (4.36).

For axially symmetrical fiber arrangement at an angle θ with respect to the x_1 axis, the fiber orientation effect can be investigated as in Section 4.3.2. By transforming the effective thermal conductivity tensor k_{ij} based upon the $[T]$ matrix of Eq. (4.17) and subsequently integrating the tensor components over the 2π range of φ, the resulting components are transversely isotropic with respect to the x_2–x_3 plane:

$$
\begin{aligned}
k_{11}^* &= k_{11}\cos^2\theta + k_{22}\sin^2\theta \\
k_{22}^* &= k_{33}^* = \tfrac{1}{2}k_{11}\sin^2\theta + k_{22}\left(\frac{1+\cos^2\theta}{2}\right)
\end{aligned}
\tag{4.38}
$$

By substituting the bounds of k_{ij} (Eqs. (4.32) and (4.33)) into the above expressions, the bounds of thermal conductivity can be expressed as functions of fiber orientation θ. Again, Eq. (4.18) can be used to find the effective thermal conductivity of a composite with a given $\eta(\theta)$.

For completely random fiber orientation, the result can be simplified to

$$
k_{11}^* = k_{22}^* = k_{33}^* = \frac{k_{11}}{3} + \frac{2k_{22}}{3} \tag{4.39}
$$

Fig. 4.16. The variation of the upper and lower bounds of k_{11}/k_m with V_f for an E-glass/epoxy system. (After Nomura and Chou 1980.)

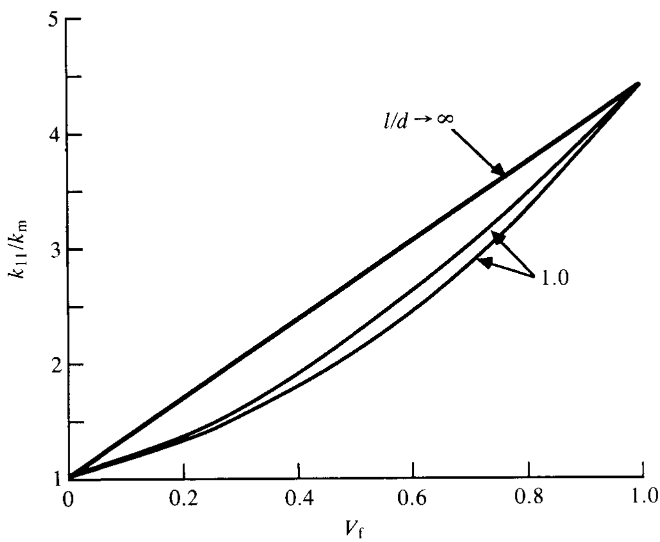

4.4.2 *Thermoelastic constants*

Knowledge of the thermoelastic constants, including thermal expansion coefficients and thermal stress coefficients, is basic to the understanding of the hygrothermal effects in composites. So far as it is assumed that these quantities obey the linear constitutive equation, their solutions can be obtained in a manner similar to the determination of effective elastic moduli or thermal conductivities. The problem of effective thermoelastic constants for non-homogeneous materials has been investigated by several researchers. The works of Kerner (1956), Levin (1967), Schapery (1968) and Budiansky (1970) are mainly concerned with composites reinforced with spherical inclusions. Rosen and Hashin (1970) extended Levin's model of a binary composite to general anisotropic composites by adopting a variational approach. Laws (1973) studied the thermoelastic behavior of anisotropic composites based upon Hill's self-consistent approximation.

By focussing attention on thermostatics and considering composites at uniform temperature, heat conduction can be excluded and the problem is uncoupled with that given in Section 4.4.1. Consider a composite subjected to a stress field, σ, and a uniform temperature rise, ΔT. The total strain of the elastic medium is given as

$$\varepsilon = \mathbf{S}\sigma + \alpha\Delta T \tag{4.40}$$

where $\mathbf{S}$ denotes the elastic compliance tensor, and α is the thermal expansion coefficient. The constitutive relation of the thermal elastic field can also be expressed in the following general form:

$$\sigma = \mathbf{C}(\varepsilon - \alpha\Delta T) \tag{4.41}$$

where $\mathbf{C}$ is the elastic stiffness tensor.

Nomura and Chou (1981) have shown that for composites reinforced with ellipsoidal inclusions and exhibiting statistical homogeneity, the effective thermoelastic constants can be evaluated following the technique for deriving elastic moduli. Figure 4.17 shows the variation of α_{ij} (normalized by the fiber thermal expansion coefficient α_f) with V_f and fiber aspect ratio l/d for a glass/epoxy system, assuming $E_f = 72.3$ GPa, $E_m = 2.76$ GPa, $\nu_m = 0.35$, $\nu_f = 0.2$, $\alpha_m = 36 \times 10^{-6}/°C$ and $\alpha_f = 5.04 \times 10^{-6}/°C$. At a given fiber volume fraction, the thermal expansion coefficient along the fiber direction (α_{11}) is smaller than that transverse to the fiber direction (α_{22}). Figure 4.18 shows a comparison of the theoretical

Fig. 4.17. The variation of α_{ij}/α_f with V_f and l/d for an E-glass/epoxy system. —— $l/d = 1$; — · — $l/d = 5$; - - - - $l/d = \infty$. (After Nomura and Chou 1981.)

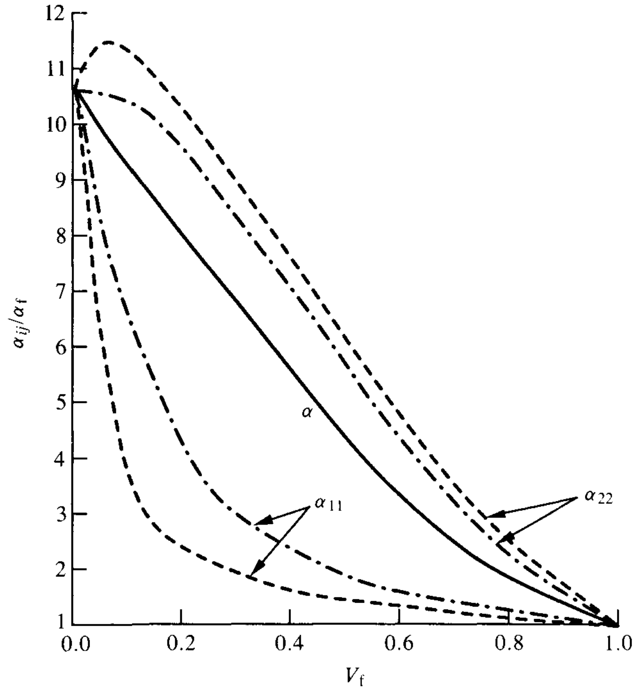

Fig. 4.18. Comparison of the predicted α_{22}/α_f with experimental data of Yates *et al.* (1978).

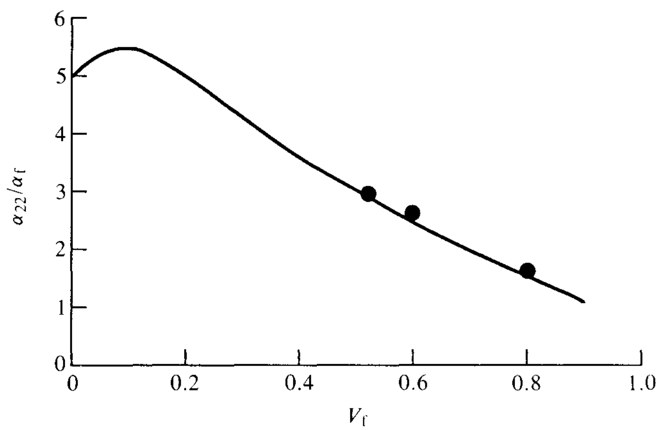

prediction of Nomura and Chou with the experimental results of Yates *et al.* (1978) on a carbon/epoxy system where $E_f/E_m = 53.4$, $\nu_m = \nu_f = 0.34$, $\alpha_m = 5 \times 10^{-5}/°C$ and $\alpha_f = 0.5–1.9 \times 10^{-5}/°C$.

4.5 Viscoelastic properties

The viscoelastic properties of composite materials were first examined by Hashin (1965b, 1969, 1972), who dealt with matrices reinforced with spherical inclusions and continuous fibers. Hashin showed that viscoelastic problems in composite materials can be solved by considering the corresponding problems in elasticity. Although application of the elastic–viscoelastic correspondence principle (see, for example, Christensen 1971) is well known, there are practical difficulties. This is due to the fact that very often the creep compliances or relaxation moduli of the constituents of a multi-component system are not known, and, even if they are given, the inverse transformation process would be formidable. Approximate methods for inverting the Laplace transform have been proposed by Schapery (1967, 1974).

The work of Laws and McLaughlin (1978) on viscoelastic composite materials adopted a self-consistent approximation. They derived the creep compliance, and numerical calculations were performed for the limiting cases of composites containing spherical inclusions and continuous fibers. Eimer (1971) derived formal effective relaxation moduli expressions of multi-phase media by considering the many point correlation functions.

Chou and Nomura (1980) and Nomura and Chou (1985) obtained the effective relaxation moduli of short-fiber composites based upon their work on effective elastic properties. Explicit expressions of composite relaxation moduli are given in terms of the elastic and viscoelastic properties of the constituent phases, fiber volume fraction, and fiber aspect ratio. Numerical calculations for a typical glass/epoxy composite system based upon the collocation approximation method as well as the self-consistent model have been performed by Nomura and Chou. It is assumed that the fiber is elastic while the matrix phase is viscoelastic. Figure 4.19 shows the time dependence of the effective axial Young's modulus of relaxation (normalized by the initial value of the matrix Young's modulus) for the fiber volume fraction of $V_f = 0.2$ and fiber aspect ratios $l/d = 5$ and ∞. The matrix behavior is shown by the lowermost curve in Fig. 4.19. The effective axial Young's modulus of relaxation at each fiber aspect ratio is calculated from the effective relaxation moduli (upper curve), the self-consistent model (middle curve), and the effective creep compliances (lower curve). The self-consistent approximation always lies in between the predictions of the two other approaches. The results also indicate that the increase in fiber length or aspect ratio makes the effective axial Young's modulus of relaxation less sensitive to the time effect. The fiber length effect also has been examined by Nomura and Chou for other effective moduli, i.e. the transverse Young's modulus of relaxation and the shear relaxation modulus, and they found no such sensitivity for these effective relaxation moduli, as in the elastic case.

4.6 Strength

Unlike continuous-fiber composites the mechanical behavior of short-fiber composites is often dominated by complex stress distributions due to fiber discontinuities. In particular, the local stress concentration at fiber ends plays a critical role in affecting the performance of short-fiber composites, and it often reduces the strength of a short-fiber composite to a level far less than that of a continuous-fiber composite with the same fiber volume content. Several theories (see Vinson and Chou 1975) have been proposed to predict the strength of discontinuous-fiber com-

Fig. 4.19. Time dependence of effective axial Young's modulus E_L/E_m for $l/d = 5$ and ∞ and $V_f = 0.2$. The viscoelastic material properties are $E_m(t) = E_m(0) = 3.2$ GPa, $E_m(\infty) = 0.04$ GPa, $\nu_m(0) = 0.365$, $\nu_m(\infty) = 0.485$, $E_f = 71.5$ GPa and $\nu_f = 0.2$. t denotes time. For each l/d value, the upper, middle and lower curves are obtained from the effective relaxation moduli, self-consistent model and effective creep compliances, respectively. (After Nomura and Chou 1985.)

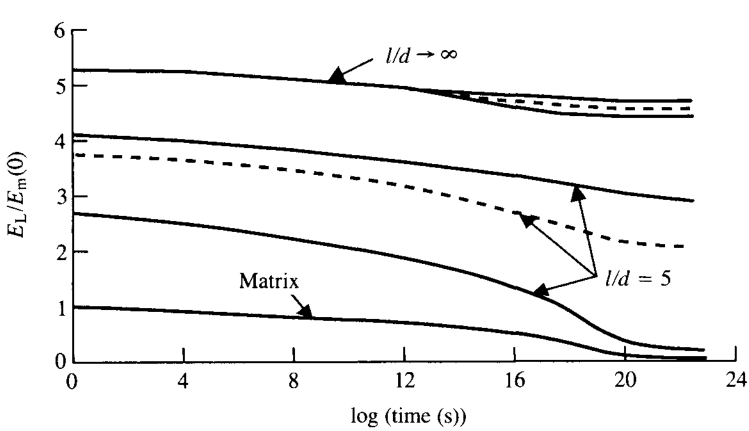

posites. One type of theory is based on a modification of the 'rule-of-mixtures', which was originally developed for continuous-fiber composites. Since the axial stress distribution in a short fiber is not uniform, the rule-of-mixtures has been modified by researchers to take into account the effect of fiber length.

Among short-fiber composites, aligned-fiber composites have many attractive properties (see Edward and Evans 1980; Richter 1980; Manders and Chou 1982). When complicated shapes and double curvatures are fabricated by matched-die molding techniques, aligned short-fiber composites have an advantage over their equivalent continuous mats (Kacir and Narkis 1975). The ability of aligned-fiber composites to elongate both parallel and perpendicular to the fiber direction without splitting complements the predominant shear deformation of woven materials. Because of their useful properties, highly aligned short-fiber composites have been commercially produced by the centrifuge (Edward and Evans 1980) and hydrodynamic alignment (Richter 1980) processes.

In the following, the strength of short-fiber composites is discussed first for the case of aligned fibers. Then, the effect of fiber orientation is considered for partially aligned and random fiber arrangements.

4.6.1 *Unidirectionally aligned short-fiber composites*

To examine the strength of short-fiber composites it is necessary to recall the original strength predictions developed by Kelly and co-workers (see Kelly and Davies 1965; Kelly and Tyson 1965a&b; Kelly 1971; Hale and Kelly 1972) for continuous-fiber composites. The ultimate axial tensile strength expression of Kelly *et al.* is (see Section 3.2)

$$\sigma_{cu} = \sigma_{fu} V_f + \sigma'_{mu}(1 - V_f) \tag{4.42}$$

where σ_{cu} and σ_{fu} are the ultimate tensile strengths of the composite and the fiber, respectively. σ_{fu} is identical with the fracture strength of brittle fibers. σ'_{mu} denotes the stress in the matrix at the failure strain of the composite.

Equation (4.42) was derived based upon the assumptions that the tensile strain in the composite is uniform along the axial direction and the applied load is distributed among the fibers and the matrix. When fibers are discontinuous, the iso-strain condition of Eq. (4.42) is no longer valid. The difference of the strains in the fiber and matrix near a fiber end induces shear stresses along the fiber axis.

The shear forces acting near both ends of a fiber stress the fiber in tension or compression. It is through this transferring of stress that applied load can be dispersed among the short fibers.

4.6.1.1 *Fiber length considerations*

Figure 4.20 shows schematically the variation of fiber axial tensile stress with fiber length. The profile of linear stress variation from fiber ends originates from the assumption of constant interfacial shear stress. The fiber critical length l_c is defined as the minimum fiber length necessary to build up the axial stress to σ_{fu}. The ultimate strength of a short fiber can be realized if its length reaches l_c.

Kelly and Tyson (1965a) proposed a linear transfer of stress from the tip of a fiber to a maximum value when the strain in the fiber is equal to that in the matrix. By assuming constant interfacial stress τ, the fiber critical length can be easily derived by considering the balance of tensile and shear stresses:

$$\frac{l_c}{d} = \frac{\sigma_{fu}}{2\tau} \tag{4.43}$$

τ is the shear strength of either the matrix or the interface, whichever is smaller. Experimental measurement techniques for l_c have been discussed by Vinson and Chou (1975).

Using the concept of critical fiber length and replacing σ_{fu} in Eq. (4.42) by the average fiber stress $\bar{\sigma}_f$, Kelly (1973) derived the following expression of composite strength for $l \geq l_c$:

$$\begin{aligned} \sigma_{cu} &= \bar{\sigma}_f V_f + \sigma'_{mu}(1 - V_f) \\ &= \sigma_{fu}[1 - (1 - \delta)l_c/l] + \sigma'_{mu}(1 - V_f) \end{aligned} \tag{4.44}$$

where δ is defined as the ratio of the area under the stress distribution curve over the length $l_c/2$ in Fig. 4.20 to the area of

Fig. 4.20. Variations of fiber tensile stress with fiber length.

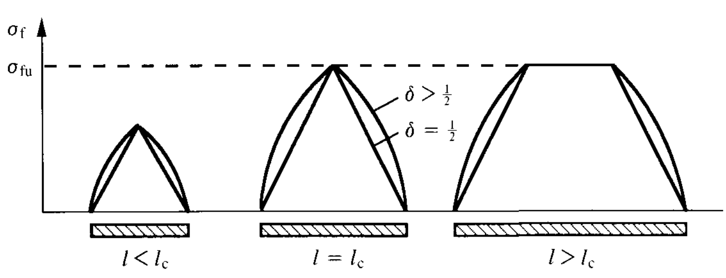

$\sigma_{fu}l_c/2$. For constant interfacial shear strength, $\delta = \frac{1}{2}$ and

$$\begin{aligned} \sigma_{cu} &= \sigma_{fu}(1 - l_c/2l)V_f + \sigma'_{mu}(1 - V_f) \qquad l \geq l_c \\ \sigma_{cu} &= \sigma_{fu} V_f l/2l_c + \sigma'_{mu}(1 - V_f) \qquad l \leq l_c \end{aligned} \tag{4.45}$$

Equations (4.45) predict that for short fibers with $l/l_c = 10$, $\bar{\sigma}_f$ reaches 95% of the value for continuous fibers. Equations (4.45) have been shown to be a good approximation for metallic (Kelly and Tyson 1965a&b; Kelly 1973) and polymer matrices (Kelly 1973; Riley and Reddaway 1968; Hancock and Cuthbertson 1970). It should be noted that Eqs. (4.45) do not consider fiber end stress concentration which occurs in short-fiber composites. There exist several variants of Kelly's formulation of short-fiber composite strength. For example, Outwater (1956) has taken into consideration the effect of interfacial friction load due to resin cure shrinkage. However, there lies the difficulty of measuring the friction coefficient and radial shrinkage pressure (Kardos 1973).

For pure elastic deformation of the fiber, $\sigma_{fu} = E_f\varepsilon_{cu}$ where ε_{cu} is the composite ultimate strain. Equation (4.43) can be rewritten as

$$\frac{l_c}{d} = \frac{E_f\varepsilon_{cu}}{2\tau} \tag{4.46}$$

For composites with variation in fiber length, Bowyer and Bader (1972) pointed out that at any value of composite strain ε_c there is a critical fiber length given by

$$l_\varepsilon = \frac{E_f\varepsilon_c d}{2\tau} \tag{4.47}$$

Fibers shorter than l_ε will carry the average stress

$$\bar{\sigma}_f = \frac{l\tau}{d} \tag{4.48}$$

which is always less than $\frac{1}{2}E_f\varepsilon_c$. Fibers longer than l_ε carry the average stress

$$\bar{\sigma}_f = E_f\varepsilon_c\left(1 - \frac{E_f\varepsilon_c d}{4l\tau}\right) \tag{4.49}$$

which is always greater than $\frac{1}{2}E_f\varepsilon_c$.

Following Bowyer and Bader, for a composite containing a spectrum of fibers of different lengths, its strength can be estimated by dividing the length of fibers into sub-fractions at a given composite strain level (Lees 1968). Sub-critical fractions are denoted by l_i and their respective volume fractions V_i while super-critical fractions are denoted by l_j and V_j. Thus the composite stress can be expressed as

$$\sigma_c = \sum_i^{l_i<l_\varepsilon} \frac{\tau l_i V_i}{d} + \sum_j^{l_j>l_\varepsilon} E_f \varepsilon_c \left(1 - \frac{E_f \varepsilon_c d}{4 l_j \tau}\right) V_j + E_m \varepsilon_c (1 - V_f) \quad (4.50)$$

Equation (4.47) indicates that at low composite strain l_ε is small and all fibers will contribute to the reinforcement as given by Eq. (4.49). As the strain is increased, a progressively smaller proportion of the fibers will reinforce according to Eq. (4.49) and an increasing proportion will follow Eq. (4.48). Thus, the load-extension curve for such a material as indicated by Eq. (4.50) is expected to show smaller slope as the strain is increased. The work of Bowyer and Bader on short-fiber-reinforced thermoplastics has further shown that improvements in the fiber–matrix bond strength have led to small improvements in strength. Also the fibers which are too short to be strained coherently with the matrix tend to fail at very low strains preventing the potential of the longer fibers from being realized. Thus the very short fibers should be eliminated if full strengthening potential is to be achieved.

4.6.1.2 *Probabilistic strength theory*

The following discussions of the probabilistic strength theory of short-fiber composites begin with a consideration of fiber length variations and their effect on fiber axial stress distribution. Then, the influence of local stress concentrations due to fiber–fiber interaction is introduced. A probabilistic strength theory is developed to consider the maximum stress concentration induced by the clustering of ends of short fibers.

(A) Modification of the rule-of-mixtures

Consider a unidirectional short-fiber composite material with fibers of uniform length and strength. The mechanisms of failure can be categorized according to fiber length (Fig. 4.21). When fibers are very short, a crack formed at a fiber end can circumvent the neighboring fibers without breaking them (Fig. 4.21a). Final failure of the composite is then attributed to fiber pull-out. On the other hand, if fibers are sufficiently long, fiber end cracks will cause fracture of the neighboring fibers and, hence, failure of the composite (Fig. 4.21b). The strength model of Fukada

Fig. 4.21. Two failure modes in short-fiber composites. (After Fukuda and Chou 1981b.)

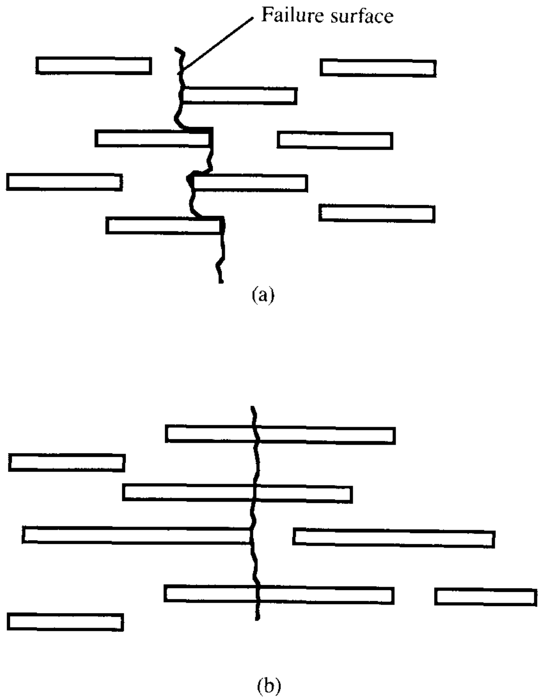

Fig. 4.22. Stress distribution in a short fiber. (After Fukuda and Chou 1981b).

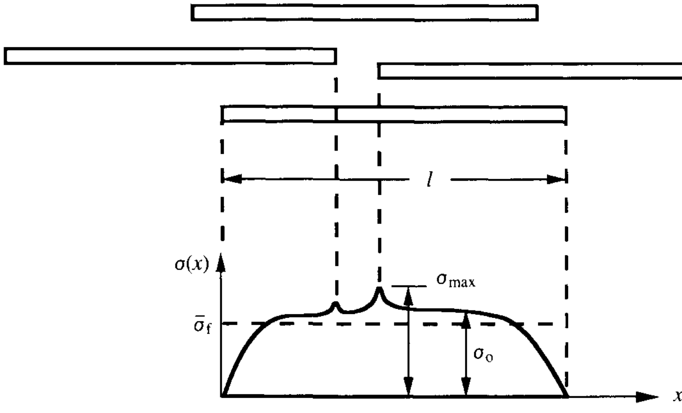

and Chou (1981a&b), and Hikami and Chou (1984a&b) aim at the latter case.

The composite ultimate strength σ_{cu} is defined as the stress level which causes first fiber fracture. Consequently, the maximum stress in a fiber is of primary importance in predicting composite strength. Figure 4.22 shows schematically stress distributions in a short fiber. Here σ_{max} and σ_o are, respectively, the maximum and plateau stress of the profile. The average fiber stress at failure is given by

$$\bar{\sigma}_f = \frac{1}{l}\int_0^l \sigma(x)\,dx \tag{4.51}$$

In the case the composite has a distribution of fiber length, Eq. (4.51) should be replaced by

$$\bar{\sigma}_f = \int_0^\infty f(l)\left\{\frac{1}{l}\int_0^l \sigma(x)\,dx\right\}dl \tag{4.52}$$

where $f(l)$ is a probability density function of fiber length and has the following characteristics:

$$\int_0^\infty f(l)\,dl = 1 \tag{4.53}$$

$$\int_0^\infty f(l)l\,dl = \bar{l} \tag{4.54}$$

$\bar{l}$ in Eq. (4.54) denotes the average fiber length. Then $\bar{\sigma}_f$ of Eq. (4.52) should be used in the rule-of-mixtures expression of Eq. (4.44). The values of $\bar{\sigma}_f$ and σ_o are not the same. However, the difference diminishes as the fiber length increases. For relatively large fiber aspect ratios it is reasonable to assume $\bar{\sigma}_f \approx \sigma_o$. Furthermore, by defining the stress concentration factor K in the following expression:

$$\sigma_{max} = \sigma_{fu} = K\sigma_o \tag{4.55}$$

Eq. (4.44) can be written as

$$\sigma_{cu} = \frac{\sigma_{fu}}{K}V_f + \sigma'_{mu}(1 - V_f) \tag{4.56}$$

(B) Critical zone model

A systematic experimental study of short-fiber composite strength has been performed by Curtis, Bader and Bailey (1978) using polyamide thermoplastic reinforced with short glass and carbon fibers. Their experimental findings led Bader, Chou and Quigley (1979) to propose a damage model. The basic concepts are that microcracks are most likely to develop at fiber ends at microscopic strains well below the fiber failure strain, and that failure is finally initiated in a critical cross-section that has been weakened by the accumulation of cracks.

Figure 4.23 depicts a typical volume element in a short-fiber composite used by Bader, Chou and Quigley. The width of a 'critical zone' in the strength model is denoted by βl where $0 < \beta \leq 1$ is a constant parameter and l is the average fiber length. The critical zone width is assumed to be of the same order as the fiber ineffective length (Sections 3.4.6.1 and 4.2.2).

A discontinuous fiber can end in the zone (ending fiber), in which case it bears no load, or it can bridge the zone (bridging fiber) and contribute to the strength of the critical zone. The probabilities of finding an ending fiber and a bridging fiber are β and $1-\beta$, respectively. All fibers are assumed to have uniform strength σ_{fu}. Within each transverse section of the composite, ending fibers and bridging fibers are distributed randomly. A typical fiber configuration on a transverse section in a two-dimensional fiber array is shown in Fig. 4.24. The ending fibers and bridging fibers are depicted, respectively, by solid circles and open circles. Under the applied stress, the stress in the bridging fibers is enhanced by the

Fig. 4.23. A typical critical zone in a short-fiber composite. (After Bader, Chou and Quigley 1979).

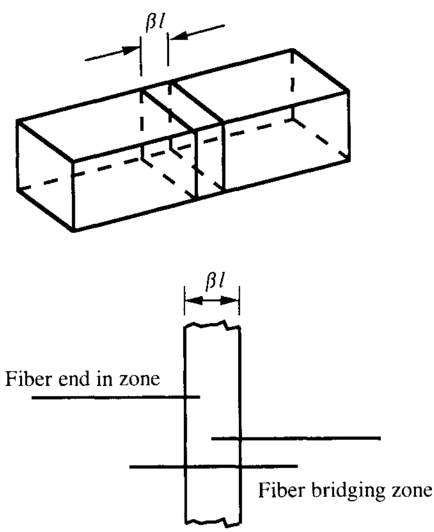

stress transferred from the neighboring ending fibers. For example, the stress in the bridging fiber no. 8 in this figure is enhanced by the ending fibers nos. 1, 5, 6, 7, 9, 12 and 13. In other words, it is enhanced by the neighboring fiber-end-gaps *A, B, C* and *D*.

The strength of the composite is determined by the relative numbers of fibers that bridge the zone vs. those with ends within the zone. These latter will develop matrix cracks when the strain exceeds a critical value. The critical situation arises when the bridging fibers are unable to sustain the load transfer due to matrix cracking and failure occurs. The critical stress and strain values for a wide range of fiber aspect ratio, fiber critical length, fiber–matrix interfacial strength and critical zone width have been evaluated by Bader, Chou and Quigley.

(C) Stress concentration

The stress concentration factor for the unidirectional fiber arrangement of Fig. 4.25 is difficult to evaluate in a precise manner. The following assumptions are adopted to facilitate the calculation of K: (a) fibers are of the same length, l; (b) they are arranged in rows along the axial direction; (c) the spacing between two neighboring rows is uniform (Fig. 4.25a); and (d) fibers with ends in the critical zone of width βl are assumed to have the ends aligned along the cross-section zz' (Fig. 4.25b). This collection of fiber ends is termed a 'fiber-end-gap' in a two-dimensional array. It is assumed that the fiber length l is much larger than the critical length l_c and, hence, results for stress concentrations due to the fracture of long fibers can be used. Also, in Fig. 4.25(a), the number 1 and number 4 fibers are labeled as 'bridging fibers' and the number 2 and number 3 fibers as 'ending fibers'.

Since the stress concentration factor, K, cannot be readily calculated by considering the enhancement effect from all the fiber-end-gaps, assumptions need to be introduced for the load sharing rule. Hikami and Chou (1984a) have examined the first and

Fig. 4.24. Schematic cross-sectional view of fiber configuration. Solid circles depict ending fibers and open circles indicate bridging fibers. A group of adjacent ending fibers is termed a fiber-end-gap (i.e. *A, B, C* and *D*). (After Hikami and Chou 1984a.)

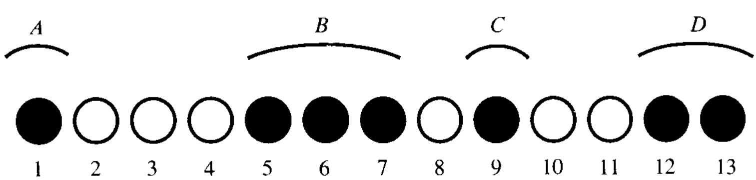

simplest approximation for K by only considering the stress enhancement effects of the first nearest neighboring fiber-end-gap of a bridging fiber. This is known as the *weak local load sharing rule* and the assumption is allowable if the probability of finding the ending fibers is relatively small. Using the shear-lag method, the stress concentration factor due to the presence of n_l and n_r ending fibers (Fig. 4.26) has been obtained by Hikami and Chou (1984a and b, 1990).

It can be shown that the failure of the $(n_l + 1)$th fiber does not cause the composite failure since the stress concentration factor for the $(n_l + 1)$th fiber is larger than that for the zeroth bridging fiber after the failure of the $(n_l + 1)$th bridging fiber. Clearly, the failure of the zeroth bridging fiber causes the total failure of the composite. Thus neglecting the load bearing capacity of the matrix, the strength of the composite is given by

$$\sigma_{cu} = \sigma_{fu}/K_b \tag{4.57}$$

The explicit expression of elastic stress concentration factor K_b due to b broken fibers is given in Section 3.3.1.2.

Fig. 4.25. (a) Critical zone in a two-dimensional fiber array. (b) A fiber-end-gap. (After Fukuda and Chou 1981b.)

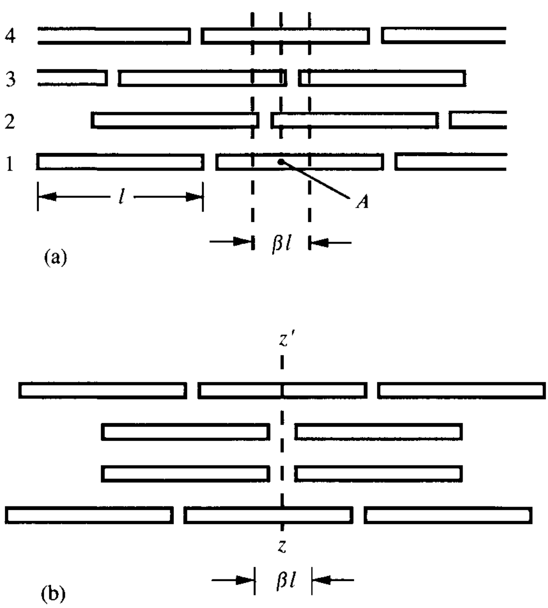

The explicit expression of stress concentration factor for composites with plastically deformed matrices (Fig. 4.26) has also been obtained by Hikami and Chou (1984a). For the small-scale plastic deformation case, the plastic stress concentration factor, $\tilde{K}_b$, can be expressed in series expansion form in terms of the dimensionless plastic deformation zone length α.

In the large-scale plastic deformation case, $\tilde{K}_b$ at the tip of a fiber-end-gap can be approximated by

$$\tilde{K}_b \cong 1 + \frac{2}{\pi}\left(\frac{T_o}{\sigma_a}\right)[nl(b\sigma_a/T_o) + \gamma'] \tag{4.58}$$

where

$$T_o = \tau_m \sqrt{(hE_f/G_m A_f)} \tag{4.59}$$

Fig. 4.26. Model of stress concentration calculations for a fiber-end-gap in short-fiber composites with matrix plastic deformation zone at the tip of the gap. (After Hikami and Chou 1984.)

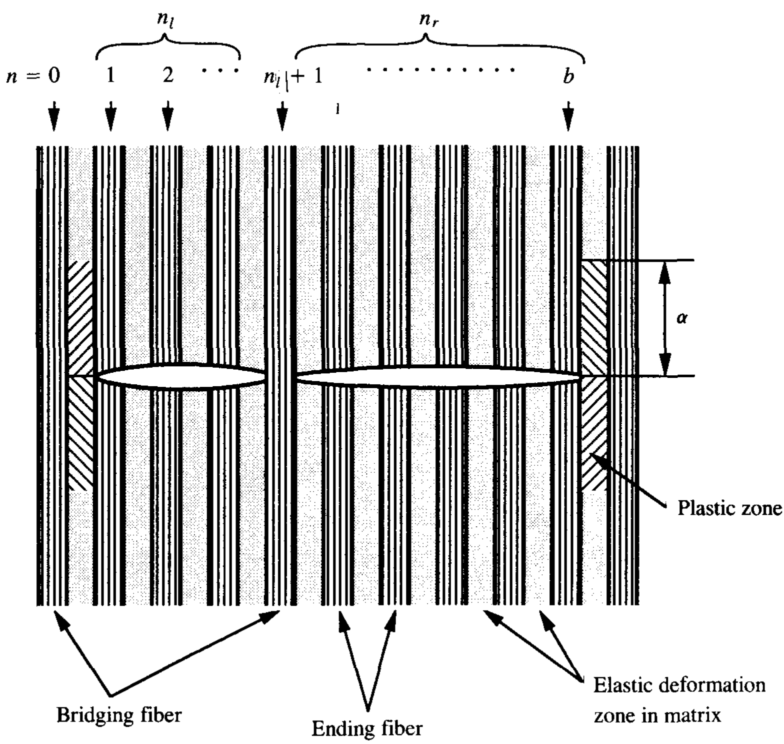

Also, σ_a = applied stress, b = number of fibers in the gap, γ' = Euler's constant ($\approx$0.577), τ_m = matrix shear strength, G_m = matrix shear modulus, E_f = fiber axial Young's modulus, h = fiber spacing, and A_f = fiber cross-sectional area. The fibers are of unit thickness.

(D) Probability distribution of maximum fiber-end-gap

The fiber-end-gap size has been analyzed by Hikami and Chou (1984a) for the case of the two-dimensional array shown in Fig. 4.25(b). Focussing attention on a single fiber end, the probability, P_n, that this fiber end is in the gap consisting of n fiber ends is

$$P_n = n\beta^{n-1}(1-\beta)^2 \tag{4.60}$$

and

$$\sum_{n=1}^{\infty} P_n = 1 \tag{4.61}$$

The probability that a given fiber end is not in any one of the gaps with more than n fiber ends is

$$Q_n = 1 - \sum_{i=n+1}^{\infty} P_i \tag{4.62}$$

When the above probability is independent for each fiber, the probability that there is no gap larger than size n is

$$\tilde{P}(n) = (Q_n)^N \tag{4.63}$$

where N is the total number of fibers in the composite. However, actually Q_n for a given fiber is not independent of the other fibers. When N is sufficiently larger than the average gap size, $\bar{n}$, it is more suitable to express $\tilde{P}(n)$ of Eq. (4.63) as

$$\tilde{P}(n) = (Q_n)^{N/\bar{n}} \tag{4.64}$$

where

$$\bar{n} = \sum_{n=1}^{\infty} nP_n \tag{4.65}$$

Using Eqs. (4.60) and (4.62), Eq. (4.64) can be rewritten as

$$\tilde{P}(n) = \{1 - \beta^n[n(1-\beta)+1]\}^{N\beta'} \tag{4.66}$$

and

$$\beta' = \frac{1}{\bar{n}} = \frac{1-\beta}{1+\beta} \tag{4.67}$$

$\tilde{P}(n)$ can be used to determine the strength of short-fiber composites through the relation between gap size, n, and the corresponding stress concentration. Figure 4.27 demonstrates the variation of $\tilde{P}(n)$ with N and β. It can be shown that $\tilde{P}(n)$ behaves like a step function and $\tilde{P}(n)$ changes from 0 to 1 at $n \cong M$, where M is determined from

$$\beta^n[n(1-\beta)+1]N\beta' = 1 \tag{4.68}$$

M obtained from Eq. (4.68) is termed the 'most probable maximum gap size'. Figure 4.28 shows M as a function of β and N. For actual composites, the values of M do not vary tremendously with β and N. When N is sufficiently large, using the formula $1-x \cong \exp(-x)$, $\tilde{P}(n)$ can be approximated as

$$\tilde{P}(n) \cong \exp[-N\beta^n n(1-\beta)^2] \tag{4.69}$$

(E) Strength predictions

Based upon the considerations of fiber-end-gap size and stress concentrations, Hikami and Chou (1984a) have proposed a modification of the rule-of-mixtures for composite strength. The composite ultimate strength σ_{cu} is defined as the stress level at which fracture of the composite occurs. Based upon the approxima-

Fig. 4.27. Cumulative probability distribution functions for the maximum fiber-end-gap size. ○: $N = 10^6$, $\beta = 0.2$; ●: $N = 10^6$, $\beta = 0.1$; △: $N = 10^8$, $\beta = 0.2$. (After Hikami and Chou 1984a.)

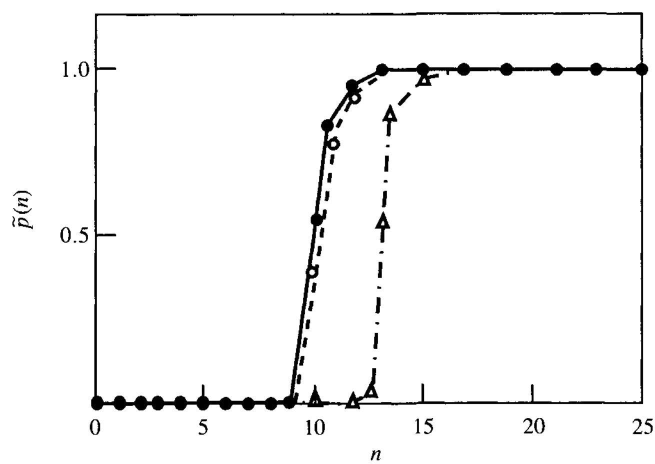

tions discussed above, σ_{cu} is given as

$$\sigma_{cu} = \sigma_a V_f + \sigma'_{mu}(1 - V_f) \tag{4.70}$$

Here, σ'_{mu} is the matrix stress at the ultimate tensile strain of the fiber. σ_a is the applied fiber stress at the instant when the fiber stress at the site of stress concentration reaches σ_{fu}. Thus, σ_a satisfies the following relation:

$$\sigma_{fu} = K[\sigma_a - \eta\sigma_{my}(1 - V_f)/V_f] \tag{4.71}$$

for the weak local load sharing rule, where $K = K_b$ or $\tilde{K}_b$. σ_{my} is the matrix yield strength. The parameter η in Eq. (4.71) reflects the loading condition of the matrix in the fiber-end-gap. If the matrix is brittle, a crack can propagate in the matrix along the fiber-end-gap prior to the failure of the intact bridging fiber. In this case, the matrix in the fiber-end-gap will bear no load and η is taken to be zero. However, in a ductile matrix composite the matrix in the fiber-end-gap can deform plastically to the yield strength, σ_{my}. Then each fiber in the fiber-end-gap sustains the stress $\sigma_{my}(1 - V_f)/V_f$, thus reducing the applied stress σ_a, and $\eta = 1$. Since the fracture of a composite initiates at the weakest point, the stress concentration factor for the most probable maximum gap size M of Eq. (4.68) should be used.

Fig. 4.28. Most probable maximum gap size, M, vs. critical zone parameter, β. N denotes the total number of fibers. (After Hikami and Chou 1984a.)

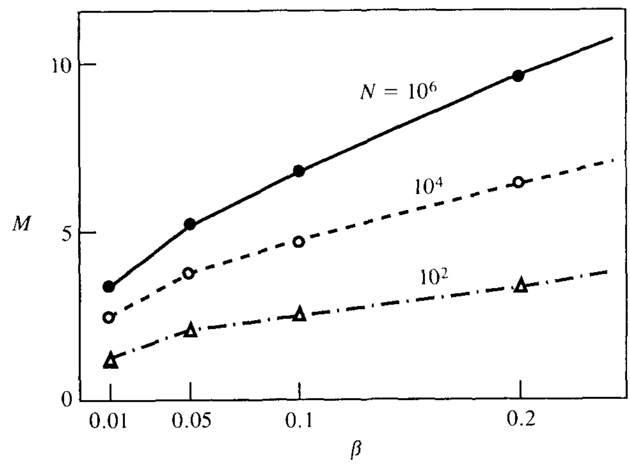

In the case of three-dimensional fiber arrays, the problem is more complicated and there is no rigorous probabilistic treatment available. The shape of the fiber-end-gap cannot be uniquely defined for a given number of fiber ends and it is fairly involved to obtain the highest stress concentration factor in the intact bridging fibers. Furthermore, the fiber failure process here is more complex than that in the two-dimensional case. To circumvent these difficulties, Fukuda and Chou (1981b) took only compact fiber-end-gaps as the first approximation. Following this approximation, Hikami and Chou (1984a) have considered the special type of fiber-end-gap which consists of square-arrayed ending fibers. A typical example of such a fiber-end-gap is shown in Fig. 4.29, where ending fibers are indicated by solid circles and bridging fibers by open circles in the two-dimensional square lattice. Approximations for the most probable maximum gap size and the resulting composite strength have been obtained and the details can be found in the reference.

The relation between the fiber volume fraction, V_f, and composite strength normalized by the matrix stress at failure, σ_{cu}/σ'_{mu}, is shown in Fig. 4.30 for the case of an elastic matrix. The properties of a glass fiber/thermoplastic matrix composite are used; fiber length $(l) = 1$ mm; fiber diameter $(d) = 0.01$ mm; fiber critical length $(l_c) = 0.1$ mm; and critical zone parameter $(\beta) = 0.1$. Also $\sigma_{fu}/\sigma'_{mu} = E_f/E_m = 35.2$.

In Fig. 4.30, line A shows the simple rule-of-mixtures for continuous fibers, while line B depicts the rule-of-mixtures modified for short fibers. Neither case takes the effect of local stress

Fig. 4.29. Schematic cross-sectional view of a three-dimensional fiber array. Solid circles indicate ending fibers and open circles are for bridging fibers. (After Hikami and Chou 1984a.)

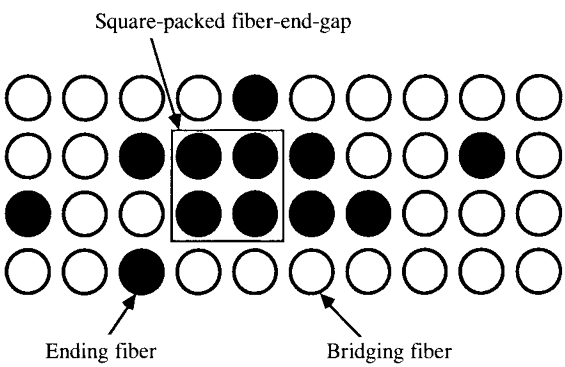

concentrations into consideration. Lines C and E indicate the results of Hikami and Chou (1984a) for a three-dimensional fiber array and a two-dimensional fiber array, respectively, based on the local load sharing rule. The composite strength is expected to lie between these two bounds, which are far less than the values obtained from the rule-of-mixtures because of local stress concentrations.

4.6.2 *Partially oriented short-fiber composites*

Cox (1952) first proposed the idea of orientation factor in the strength equation for continuous fiber composites to account for fiber misalignment. Bowyer and Bader (1972) adopted this concept in their study of short-fiber systems, and Eq. (4.50) was modified by multiplying the fiber dependent terms on the right-hand side of this equation by the orientation factor C_o, $C_o = 1$ for perfectly aligned fibers and C_o assumes values less than unity for partially oriented fibers. Bowyer and Bader concluded that the orientation factor is independent of strain and is the same for all fiber length at least at small strains. The orientation factor can then be calculated from Eq. (4.50) based upon the knowledge of fiber length distribution, interfacial bond strength and composite ultimate tensile strength.

Curtis, Bader and Bailey (1978) investigated the strength of a

Fig. 4.30. Strength of the composite as a function of V_f. A: rule-of-mixtures; B: Kelly and Tyson (1965b); C: three-dimensional fiber array, weak local load sharing; E: two-dimensional fiber array, weak local load sharing. (After Hikami and Chou 1984a.)

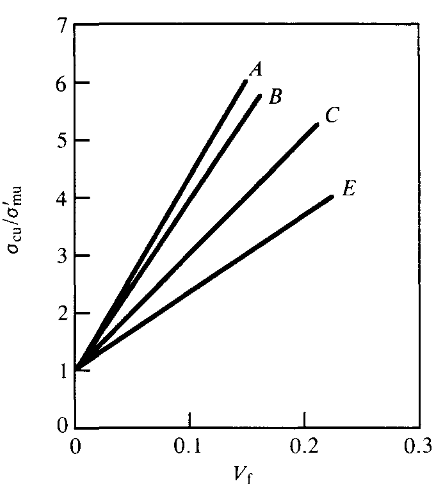

polyamide thermoplastic reinforced with glass and carbon fibers, and calculated the fiber orientation factor from the measured composite modulus and the knowledge of the fiber and matrix properties. Their results indicate that fiber alignment increases with increasing fiber volume fraction, which agrees with the qualitative assessment of optical micrographs.

In general, when there are variations in both fiber length and orientation, the rule-of-mixtures (Eq. (4.42)) can be modified as

$$\sigma_{cu} = \sigma_{fu} V_f F(l_c/\bar{l}) C_o + \sigma'_{mu}(1 - V_f) \tag{4.72}$$

Here, the factor $F(l_c/\bar{l})$ is a function of fiber average length $\bar{l}$ and critical length l_c. Equations (4.45), for instance, give the forms of $F(l_c/\bar{l})$ for aligned short fibers of uniform length. If the necessary information with respect to fiber orientation is known, C_o can be estimated analytically.

Fukuda and Chou (1982) have used a probabilistic theory to predict the strength of short-fiber composites with variable fiber length and orientation. They introduced two kinds of probability density functions to describe the fiber length and orientation distributions and neglected the effect of stress concentration in this particular treatment. The analytical result of composite strength is given only in the form of an average value. The theory of Fukuda and Chou is introduced below in three parts.

(A) Geometrical consideration of a single short fiber

First, the geometrical arrangement of a single short fiber is described. Figure 4.31(a) shows an obliquely positioned short fiber

Fig. 4.31. Several notations on short-fiber arrangement. (a) Obliquely oriented fiber. (b) Bridging fiber and ending fiber. (c) Critical angle. (After Fukuda and Chou 1982.)

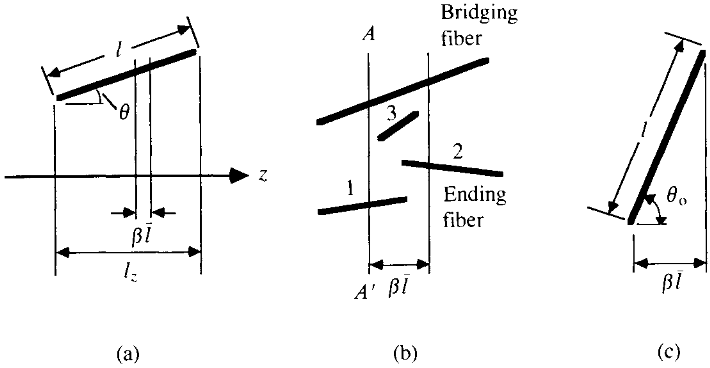

of length l. In accordance with the terminology of Section 4.6.1, a bridging fiber and an ending fiber are defined in Fig. 4.31(b); that is, if a fiber crosses a critical zone (Section 4.6.1.2) of width $\beta\bar{l}$, it is termed a bridging fiber; and if the end of a fiber is within the critical zone, it is defined as an ending fiber. Here, $\bar{l}$ denotes average fiber length. The probability density function of fiber length distribution $h(l)$ satisfies the following condition:

$$\int_0^\infty h(l)\,\mathrm{d}l = 1 \tag{4.73}$$

Then, the average fiber length is defined as

$$\bar{l} = \int_0^\infty l h(l)\,\mathrm{d}l \tag{4.74}$$

From Fig. 4.31(a),

$$l_z = l \cos\theta \tag{4.75}$$

and from Fig. 4.31(c) the critical angle θ_o within which a fiber of length l is a bridging fiber becomes

$$\theta_o = \cos^{-1} \beta\bar{l}/l \tag{4.76}$$

for $\beta\bar{l} \le l$. If $\beta\bar{l} > l$, θ_o cannot be defined, and a fiber in such a case is inevitably an ending fiber. If the fibers are distributed randomly with respect to the z axis, the probability p_e that a fiber of length l is an ending fiber in the critical zone becomes

$$p_e = \frac{\beta\bar{l}}{l_z} = \begin{cases} \beta\bar{l}/l\cos\theta & (0 \le \theta \le \theta_o \text{ and } \beta\bar{l} \le l) \\ 1 & (\theta_o \le \theta \le \pi/2 \text{ or } \beta\bar{l} \ge l) \end{cases} \tag{4.77}$$

and the probability p_b for finding a bridging fiber is, by definition,

$$p_b = 1 - p_e \tag{4.78}$$

The probability density function with respect to fiber orientation $(g(\theta))$ should satisfy the condition

$$\int_0^{\pi/2} g(\theta)\,\mathrm{d}\theta = 1 \tag{4.79}$$

(B) Load transfer in a short fiber

First, consider a short fiber situated parallel to the applied tensile stress, σ_o, along the z axis. The average fiber stress is

$$\sigma_{fo} = \frac{1}{l}\int_0^l \sigma_f(z)\,\mathrm{d}z \tag{4.80}$$

The fiber axial stress $\sigma_f(z)$ has, in general, the profile shown in Fig. 4.1. Consider the simplest form of $\sigma_f(z)$ by assuming a constant interfacial shear stress (Fig. 4.20). Then σ_{fo} becomes

$$\sigma_{fo} = \begin{cases} \sigma_{fu}\left(1 - \dfrac{l_c}{2l}\right) & (l > l_c) \\ \sigma_{fu}\left(\dfrac{l}{2l_c}\right) & (l < l_c) \end{cases} \tag{4.81}$$

The average force in a fiber of cross-sectional area A_f is $\sigma_{fo}A_f$.

Next, consider a single short fiber situated at an angle θ to the applied stress σ_o. The applied stress can be decomposed into an axial and a shear component, with respect to the fiber axis, as

$$\sigma_o' = \sigma_o \cos^2\theta \tag{4.82}$$

$$\tau_o' = \sigma_o \sin\theta \cos\theta \tag{4.83}$$

If the effect of τ_o' on the fiber stress distribution can be neglected, the average force of the fiber becomes $A_f\sigma_{fo}\cos^2\theta$ and the z direction force component is

$$F_z = A_f\sigma_{fo}\cos^3\theta \tag{4.84}$$

(C) Strength of short-fiber composites

Based upon the above preparations, the strength of short-fiber composites can be derived. In the following discussion, $h(l)$ and $g(\theta)$ are assumed to be independent of each other. This means that $g(\theta)$ is the same for all the samples with different fiber length distributions. A rectangular-shaped specimen with the lengths of the three mutually perpendicular edges denoted by a, b and c is considered. The c axis is so chosen as to be parallel to the z axis. The volume of the specimen is

$$V = abc \tag{4.85}$$

and from the definition of fiber volume fraction, V_f becomes

$$V_f = NA_f\bar{l}/V \tag{4.86}$$

where N and A_f denote, respectively, the total number of fibers and fiber cross-sectional area.

Recall that Eq. (4.76) gives the length of the projection of a fiber on the z axis. Then the average length of the projection of fibers can be written as

$$\bar{l}_z = \int_0^{\pi/2} \int_0^{\infty} l \cos\theta \, h(l) g(\theta) \, \mathrm{d}l \, \mathrm{d}\theta$$
$$= \bar{l} \int_0^{\pi/2} g(\theta) \cos\theta \, \mathrm{d}\theta \tag{4.87}$$

The value of $N\bar{l}_z$ gives the total length of projection of all fibers on the z axis and if this value is divided by the specimen length c, the average number of fibers which cross an arbitrary section in the specimen normal to the z axis is obtained. That is,

$$N_c = \frac{N\bar{l}_z}{c} = \frac{abV_f}{A_f} \int_0^{\pi/2} g(\theta) \cos\theta \, \mathrm{d}\theta \tag{4.88}$$

Equation (4.77) gives the probability of a specific fiber being an ending fiber. Therefore, the average probability of finding an arbitrary fiber being an ending fiber is

$$q_e = \int_0^{\pi/2} \int_0^{\infty} p_e h(l) g(\theta) \, \mathrm{d}l \, \mathrm{d}\theta \tag{4.89}$$

Similarly, the average probability of finding an arbitrary fiber being a bridging fiber is

$$q_b = \int_0^{\pi/2} \int_0^{\infty} p_b h(l) g(\theta) \, \mathrm{d}l \, \mathrm{d}\theta$$
$$= 1 - q_e \tag{4.90}$$

Substituting Eqs. (4.77) and (4.78) into Eqs. (4.89) and (4.90),

$$q_e = \int_0^{\theta_o} \mathrm{d}\theta \left(\int_0^{\beta\bar{l}} g(\theta) h(l) \, \mathrm{d}l + \int_{\beta\bar{l}}^{\infty} \frac{\beta\bar{l}}{l \cos\theta} g(\theta) h(l) \, \mathrm{d}l \right)$$
$$+ \int_{\theta_o}^{\pi/2} \int_{\beta\bar{l}}^{\infty} g(\theta) h(l) \, \mathrm{d}l \, \mathrm{d}\theta \tag{4.91}$$

$$q_b = \int_{\beta\bar{l}}^{\infty} \mathrm{d}l \int_0^{\theta_o} \left(1 - \frac{\beta\bar{l}}{l \cos\theta} \right) g(\theta) h(l) \, \mathrm{d}l \tag{4.92}$$

Then, the total numbers of ending and bridging fibers in the specimen are

$$N_e = N_c q_c \tag{4.93}$$

$$N_b = N_c q_b \tag{4.94}$$

Strictly speaking, the value of N_e is not precise because only *one* cross-section, for example AA' in Fig. 4.31(b), has been examined. The fibers denoted by 2 and 3 in Fig. 4.31(b) are not considered. However, the objective is to calculate the number of bridging fibers, which is not affected by N_e in the subsequent discussions.

Based upon Eq. (4.84) for the z direction component of the axial load of one specific fiber, the average value among the bridging fibers is

$$\bar{F}_z = \int_0^{\theta_o} \int_{\beta \bar{l}}^{\infty} F_z h(l) g(\theta)\, dl\, d\theta \tag{4.95}$$

Then the total load that all of the bridging fibers can sustain in the zone $\beta\bar{l}$ is

$$F_T = N_b \cdot \bar{F}_z \tag{4.96}$$

and the composite strength becomes

$$\sigma_{cu} = \frac{F_T}{ab} + \sigma'_{mu}(1 - V_f) \tag{4.97}$$

where the matrix is assumed to sustain part of the applied load. Substituting Eqs. (4.81), (4.84), (4.88) and (4.91)–(4.96) into Eq. (4.97), the composite ultimate strength is determined as

$$\begin{aligned}\sigma_{cu} &= \sigma_{fu} V_f \int_0^{\pi/2} g(\theta) \cos\theta\, d\theta \int_0^{\theta_o} g(\theta) \cos^3\theta\, d\theta \\ &\times \int_{\beta\bar{l}}^{\infty} \int_0^{\theta_o} \left(1 - \frac{\beta\bar{l}}{l\cos\theta}\right) g(\theta)\, d\theta\, h(l)\, dl \\ &\times \left[\int_{\beta\bar{l}}^{l_c} \frac{l}{2l_c} h(l)\, dl + \int_{l_c}^{\infty} \left(1 - \frac{l_c}{2l}\right) h(l)\, dl\right] + \sigma'_{mu}(1 - V_f)\end{aligned} \tag{4.98}$$

Equation (4.98) is a general strength expression of short-fiber composites. In order to conduct further analysis, it is necessary to know the functions $g(\theta)$ and $h(l)$ together with σ_{fu}, σ'_{mu}, V_f and l_c.

Some limiting cases of Eq. (4.98) are discussed in the following. First, consider a unidirectional short-fiber composite with uniform fiber length $\bar{l}$. Equation (4.98) can be reduced to

$$\begin{aligned}\sigma_c &= \sigma_{fu} V_f (1 - \beta)\left(1 - \frac{l_c}{2\bar{l}}\right) + \sigma'_{mu}(1 - V_f) \qquad (\bar{l} > l_c) \\ \sigma_c &= \sigma_{fu} V_f (1 - \beta)\frac{\bar{l}}{2l_c} + \sigma'_{mu}(1 - V_f) \qquad (\bar{l} < l_c)\end{aligned} \tag{4.99}$$

Equations (4.99) coincide with the result of the original failure model of Bader, Chou and Quigley (1979).

Secondly, consider the effect of fiber length distribution on the strength of a unidirectional composite. By assuming the limiting case of $\beta \to 0$, namely all fibers are bridging, and the following probability density function of fiber length distribution

$$h(l) = \frac{\pi}{4\bar{l}} \sin\left(\frac{\pi l}{2\bar{l}}\right) \qquad (0 \leq l/\bar{l} \leq 2) \tag{4.100}$$

Eq. (4.98) is reduced to

$$\sigma_{\text{cu}} = \sigma_{\text{fu}} V_{\text{f}} \left\{ \frac{1}{2} + \frac{\bar{l}}{2\pi l_{\text{c}}} \sin\left(\frac{\pi l_{\text{c}}}{2\bar{l}}\right) + \frac{1}{4}\cos\left(\frac{\pi l_{\text{c}}}{2\bar{l}}\right) - \frac{\pi l_{\text{c}}}{8\bar{l}} \left[\text{Si}(\pi) - \text{Si}\left(\frac{\pi l_{\text{c}}}{2\bar{l}}\right) \right] \right\} + \sigma'_{\text{mu}}(1 - V_{\text{f}}) \tag{4.101}$$

where $\text{Si}(x)$ is the integral sine function defined by

$$\text{Si}(x) = \int_0^x \frac{\sin t}{t}\,\text{d}t \tag{4.102}$$

The result of $F(l_{\text{c}}/\bar{l})$ from Eq. (4.101) is shown in Fig. 4.32 by the solid line. In the case of constant fiber length, the strength can be obtained from Eqs. (4.45) and the value is also shown in Fig. 4.32 by a broken line. It can be concluded from Fig. 4.32 that the strength of a composite material is reduced if the fiber length is not

Fig. 4.32. $F(l_{\text{c}}/\bar{l})$ vs. $l_{\text{c}}/\bar{l}$ —— fiber length distribution considered; – – – – fiber length assumed to be constant. (After Fukuda and Chou 1982.)

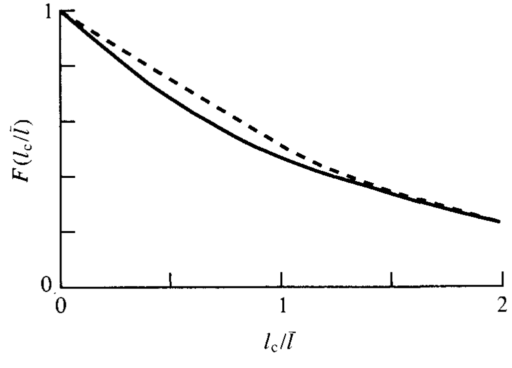

uniform. However, the difference in composite strength between the non-uniform fiber length system (Eq. (4.100)) and the uniform fiber length system is not very significant and, hence, the ordinary theory based upon an average fiber length may be used as a first approximation.

As a third example, the case of uniform fiber length and biassed fiber orientation distribution is considered. The following two types of fiber orientation are examined.

(a) $g(\theta) = 1/\alpha$ for $0 \leq \theta \leq \alpha$ and $g(\theta) = 0$ for $\theta > \alpha$;
(b) $g(\theta) = (\pi/2\alpha)\cos(\pi\theta/2\alpha)$ for $0 \leq \theta \leq \alpha$ and $g(\theta) = 0$ for $\theta > \alpha$.

These functions are taken so as to satisfy Eq. (4.79). The shapes of these functions are shown schematically in Fig. 4.33 and θ is defined in the three-dimensional view of Fig. 4.12. Note that $g(\theta)$ does not mean the probability per unit area. The probability per unit area is proportional to $g(\theta)/\sin\theta$. The limit of $\beta \to 0$ is again considered. At this limit, θ_0 tends to $\pi/2$ from Eq. (4.76). Considering this condition, C_o is calculated from Eq. (4.98) for the two types of $g(\theta)$

Fig. 4.33. Values of C_o for two types of fiber orientation distribution. (After Fukuda and Chou 1982.)

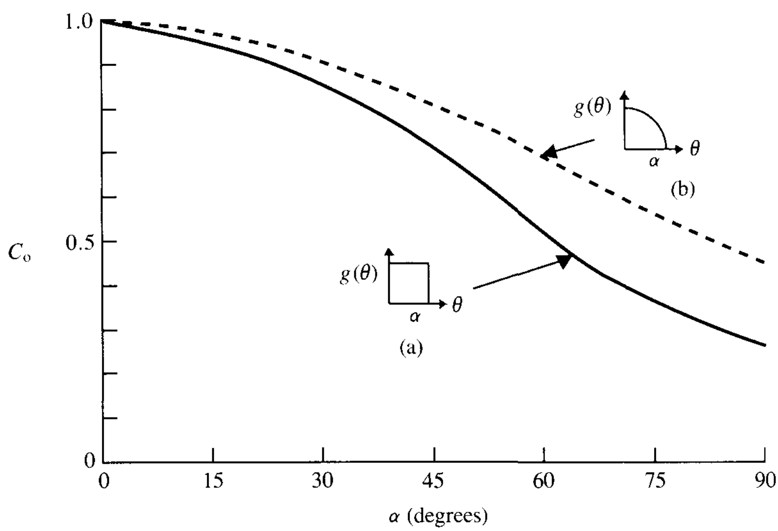

given above:

$$\text{(a)}\quad \lim_{\beta\to 0} C_o = \frac{\sin\alpha}{\alpha}\frac{1}{\alpha}\left(\frac{1}{12}\sin 3\alpha + \frac{3}{4}\sin\alpha\right)$$

$$\text{(b)}\quad \lim_{\beta\to 0} C_o = \frac{1}{16}\left[\frac{1}{1+q}\sin\frac{\pi}{2}(1+q) + \frac{1}{1-q}\sin\frac{\pi}{2}(1-q)\right] \times \left[\frac{3}{1+q}\sin\frac{\pi}{2}(1+q) + \frac{3}{1-q}\sin\frac{\pi}{2}(1-q) + \frac{1}{1+3q}\sin\frac{\pi}{2}(1+3q) + \frac{1}{1-3q}\sin\frac{\pi}{2}(1-3q)\right] \tag{4.103}$$

where $q = 2\alpha/\pi$. These values are shown in Fig. 4.33. Bowyer and Bader (1972) estimated the value of C_o by their experimental data. For laboratory glass/nylon injection molded materials, C_o was 0.66. If a retangular distribution for $g(\theta)$ is used, the value of α corresponding to $C_o = 0.66$ is approximately 45° from Fig. 4.33.

The orientation factor C_o discussed here is slightly different from the factor C_θ discussed in Section 4.3.2. The bridging effect of fibers is considered in the derivation of C_o, while the Poisson's effect of the composite is taken into account in evaluating C_θ. C_o and C_θ are essentially the same for the limiting case of $\beta \to 0$. The effect of β is discussed in Section 4.6.3.

4.6.3 *Random short-fiber composites*

Both Lees (1968a&b) and Chen (1971) attempted an averaging technique to treat the strength of random fiber composites. They adopted the failure mechanisms of Stowell and Liu (1961) and Jackson and Cratchley (1966), namely fiber failure, matrix failure in shear and matrix failure in plane strain. The operative failure mechanism in composites is dictated by the angle between the fiber direction and the direction of applied stress

$$\sigma_c = \begin{cases} \sigma_1 = \sigma_c'/\cos^2\theta & (0 \le \theta \le \theta_1) \\ \sigma_2 = \tau_m/\sin\theta\cos\theta & (\theta_1 \le \theta \le \theta_2) \\ \sigma_3 = \sigma_m/\sin^2\theta & (\theta_2 \le \theta \le \pi/2) \end{cases} \tag{4.104}$$

where σ_c' denotes the strength along the fiber direction of the unidirectional composite given by a rule-of-mixtures type of relationship. τ_m and σ_m are, respectively, the shear and tensile failure stresses of the matrix and the interface. Local stress perturbation due to fiber–fiber interaction can also be included in σ_1 of Eq.

(4.104). The strength for random fiber composites can be obtained by considering the angular strength dependence as a piecewise continuous function integrated over 90°:

$$\sigma_c = \frac{2}{\pi}\left\{\int_0^{\theta_1} \sigma_1 \, d\theta + \int_{\theta_1}^{\theta_2} \sigma_2 \, d\theta + \int_{\theta_2}^{\pi/2} \sigma_3 \, d\theta\right\} \tag{4.105}$$

The predictions of this approach agree reasonably well with experimental results on glass-reinforced polyethylene and PMMA random mat (Lees 1968a) as well as random Al_2O_3–aluminum–silicon and glass/epoxy composites (Chen 1971).

Treatments of the strength of random short-fiber composites can also be found in the works of Lee (1969), Lavengood (1972), Kardos (1973), McNally (1977) and Blumentritt, Vu and Cooper (1975). The method of laminate analogue discussed for stiffness (Section 4.3.3) can also be applied to prediction of the strength of two-dimensional random fiber composites; the strength behavior of an isotropic laminate can be simulated by unidirectionally oriented plies laid up to approximate random orientation.

The strength prediction method of Fukuda and Chou (1982) can also be applied to determine the orientation factor C_o (Eq. (4.72)) for random fiber composites. By assuming that the fiber length is uniform and is larger than the critical length l_c, Eq. (4.98) becomes

$$\sigma_{cu} = \sigma_{fu} V_f\left(1 - \frac{l_c}{2l}\right) \int_0^{\pi/2} g(\theta) \cos\theta \, d\theta \int_0^{\theta_o} g(\theta) \cos^3\theta \, d\theta \times \int_0^{\theta_o}\left(1 - \frac{\beta}{\cos\theta}\right) g(\theta) \, d\theta + \sigma'_{mu}(1 - V_f) \tag{4.106}$$

By comparing Eqs. (4.72) and (4.106), the following expression for C_o is obtained:

$$C_o = \int_0^{\pi/2} g(\theta) \cos\theta \, d\theta \int_0^{\theta_o} g(\theta) \cos^3\theta \, d\theta \times \int_0^{\theta_o}\left(1 - \frac{\beta}{\cos\theta}\right) g(\theta) \, d\theta \tag{4.107}$$

Now consider both two-dimensional and three-dimensional random fiber arrays. In a two-dimensional random array model, $g(\theta)$ must be constant in the whole region of $0 \le \theta \le \pi/2$, and

$$g(\theta) = 2/\pi \tag{4.108}$$

from Eq. (4.79). Substituting Eq. (4.108) into Eq. (4.107), the following result is obtained:

$$C_o = \frac{8}{3\pi^3}(2+\beta^2)\surd(1-\beta^2)\left[\cos^{-1}\beta - \tfrac{1}{2}\beta\log\left(\frac{1+\surd(1-\beta^2)}{1-\surd(1-\beta^2)}\right)\right] \tag{4.109}$$

The solid line of Fig. 4.34 depicts this result. As β increases, the composite contains more ending fibers and fewer bridging fibers, and hence the reinforcing effect of fibers is reduced. In the limit of $\beta \rightarrow 0$, all fibers are bridging fibers, and C_o tends to 0.27 for this two-dimensional case. Bowyer and Bader (1972) used the value of $\frac{1}{3}$ by quoting the result of Cox (1952) for the orientation factor of Young's modulus of a random composite. Cox's value is also shown in Fig. 4.34 by the solid circle.

In the case of a three-dimensional random fiber model, referring to Fig. 4.12, $g(\theta)$ can be expressed as

$$g(\theta)\,\mathrm{d}\theta = \mathrm{d}S/S$$

where the hemispherical surface area is S. Therefore,

$$g(\theta) = \sin\theta \tag{4.110}$$

Fig. 4.34. Fiber orientation factor C_o of random fiber array model. —— two-dimensional random array; – – – – three-dimensional random array. Solid and open circles indicate Cox's results. (After Fukuda and Chou 1982.)

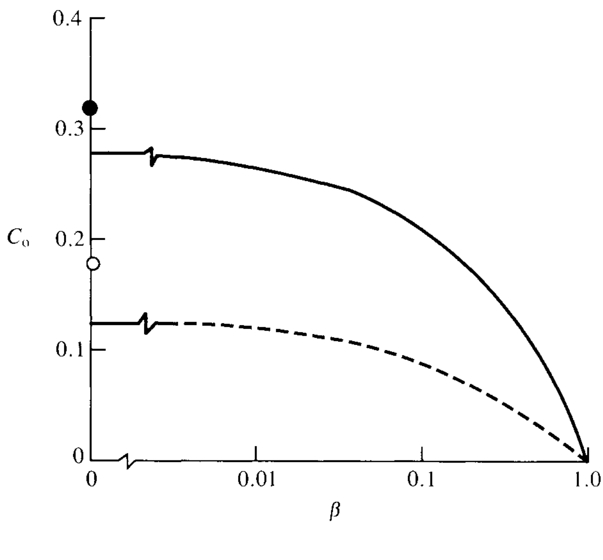

In this case, Eq. (4.107) becomes

$$C_o = \tfrac{1}{8}(1-\beta^2)(1+\beta^2)(1-\beta+\beta\log\beta) \tag{4.111}$$

This result is shown in Fig. 4.34 by a broken line. In the limit of $\beta \to 0$, C_o becomes $\frac{1}{8}$ and this value is again less than Cox's prediction of $\frac{1}{6}$ as indicated by the open circle.

4.7 Fracture behavior

Among the various types of short-fiber composites, the fracture behavior of polymer based composites is relatively well understood. The failure of short-fiber composites often initiates at microvoids and microcracks. These defects exist in the reinforcements, the matrix, and the interphase material and are introduced in the fabrication process. The final failure of a short-fiber composite is the result of several micromechanical mechanisms. The macroscopic appearance of the fracture depends on which of these mechanisms dominate the overall fracture process.

According to Friedrich (1985, 1989) and Friedrich and Karger-Kocsis (1989), the major failure mechanisms of short-fiber composites include (a) matrix deformation and fracture, (b) fiber/matrix debonding, (c) fiber pull-out, and (d) fiber fracture. A schematic fracture path through a short-fiber-reinforced polymer is given in Fig. 4.35; the individual failure mechanisms are also demonstrated.

The extent to which a specific failure mechanism occurs depends on the properties of the fiber, matrix, and interphase as well as the geometric form and arrangement of the fibers. As discussed in Sections 4.2.1 and 4.6.1, the efficiency in load transfer between a fiber and its surrounding matrix depends on the length of the fiber relative to its critical length, l_c. If the length of the fiber is shorter than l_c, fiber pull-out and matrix fracture are the dominating mechanisms of energy absorption. On the other hand, when the fiber length is longer than l_c, the fibers will, in some cases, break and in other cases be pulled out; the fiber location and orientation with respect to the crack is an important factor in determining which failure mechanism takes place.

Friedrich (1989) has examined the fracture energy of aligned short-fiber composites and given the following observations:

(1) The matrix material supplies a certain portion of the fracture energy of the composite. For a brittle polymer matrix, this portion is small in comparison to fiber fracture or interfacial failure. Then the fracture energy of the

composite as a result of fiber reinforcement is higher than that of the unfilled matrix. However, in the case of a ductile polymer matrix, the energy absorption in the fracture process is higher than those due to fiber related mechanisms. Thus, the fracture energy decreases as fiber volume fraction increases.

(2) The fiber/matrix interface shear strength, which affects the fiber critical length (Eq. (4.43)), is strongly influenced by the temperature of the environment. Higher temperatures result in higher l_c. Furthermore, the temperature also influences the matrix fracture behavior.

(3) The fracture toughness K_c of a short fiber composite is related to the fracture energy G_c and elastic modulus E by $K_c = \sqrt{(G_c E)}$. Some qualitative observations can be made concerning this relationship. First, the addition of fibers to a brittle polymer matrix enhances K_c due to a simultaneous increase in G_c and E. Second, the addition of fibers to a

Fig. 4.35. Schematic fracture path through a short-fiber-reinforced polymer, and individual mechanisms of failure: (*A*) fiber fracture, (*B*) fiber pull-out, (*C*) fiber/matrix separation, and (*D*) plastic deformation and fracture of the polymer matrix. (After Friedrich 1989.)

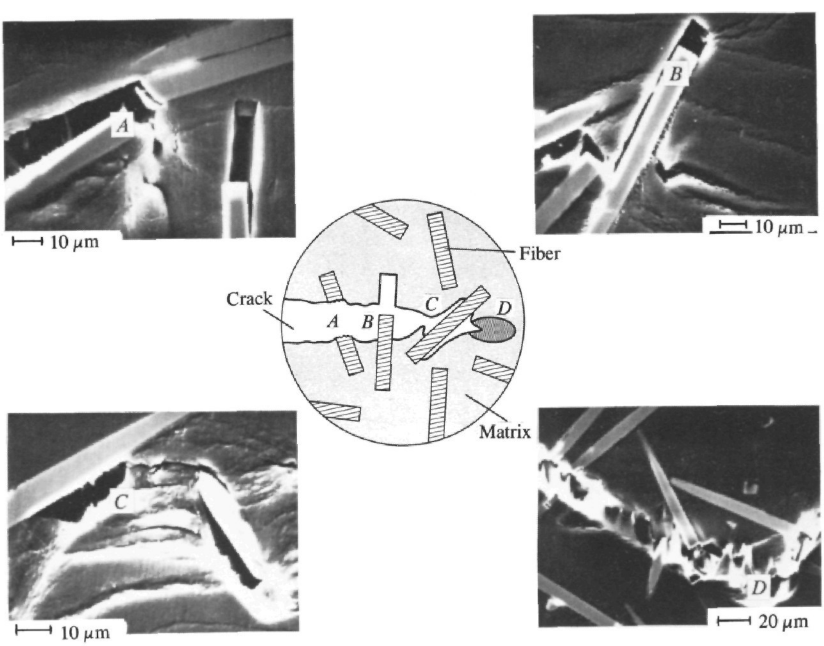

very ductile thermoplastic matrix results in an increase in E but a decrease in G_c. Thus, K_c may decrease or remain unchanged.

It is also noted that the addition of fibers can result in constraining effects on the matrix and a change of the stress state. Consequently, this leads to limited plasticity in the matrix and stress concentrations at fiber ends. The implications of the stress concentration on the fracture of short-fiber composites are discussed below.

Experimental work for identifying fiber end stress concentration was first performed by MacLaughlin (1966), who used a photoelastic method to investigate the effect of fiber end shape and gap size on the shear stress near a single short fiber. MacLaughlin (1968) extended the photoelastic study to a square-ended short fiber flanked by continuous fibers. Photoelastic methods were also used by Chen and Lavengood (1969) to examine the distribution of fiber stress and interfacial shearing stress around a short square-ended fiber.

Theoretical analyses of fiber end stress concentrations have been discussed in Section 4.2. Iremonger and Wood (1967, 1969), Muki and Sternberg (1969, 1970, 1971), Chen and Lewis (1970), Sternberg (1970), Sternberg and Muki (1970), Baker and MacLaughlin (1971) and Takao, Taya and Chou (1981) have also presented analytical solutions with particular emphasis on fiber end separation distance, fiber volume fraction, fiber and matrix modulus ratio, and fiber end geometry. Several general conclusions can be drawn from the analyses: (1) the primary parameters affecting the stress concentrations are gap size, fiber volume fraction and fiber–matrix modulus ratio; (2) square-ended and tapered-end fibers give higher stress concentrations than round-ended fibers; (3) stress concentration increases with decreasing fiber end separation distance; (4) higher stress concentrations exist at the fiber–matrix interface when the end gap is a void as compared to a gap filled with matrix. It is understood that in real composites the fiber ends are usually oblique and uneven and that the concept of fiber end separation distance is difficult to apply to a randomly distributed and misaligned fiber system. A significant finding of the stress analyses surveyed above is that the concentration of stress in the matrix near the discontinuity of a fiber is very severe even under moderate load application. Composite failure initiation, either by fracture of the matrix or by debonding, is likely to occur at these locations.

The experimental work of Curtis, Bader and Bailey (1978) on glass and carbon fiber reinforced polyamide 6.6 has demonstrated the embrittlement effect of short-fiber composites. Theoretical modeling of the fracture of short-fiber composites can be found in the work of Taya and Chou (1981, 1982), Ishikawa, Chou and Taya (1982), Takao, Chou and Taya (1982) and Takao, Taya and Chou (1982). The environmental effect on the fracture of short-fiber composites has been examined by Friedrich, Schulte, Horstenkamp and Chou (1985), Hsu, Yau and Chou (1986), and Yau and Chou (1989).